Localization and mass spectra of fermions on symmetric and asymmetric thick branes

Yu-Xiao Liu,[*,†] Chun-E Fu,[‡] Li Zhao,[§] and Yi-Shi Duan[‖]

Institute of Theoretical Physics, Lanzhou University, Lanzhou 730000, People's Republic of China

(Received 7 August 2009; published 21 September 2009)

A three-parameter (positive odd integer s, thickness factor λ, and asymmetry factor a) family of asymmetric thick brane solutions in five dimensions were constructed from a two-parameter (s and λ) family of symmetric ones in by R. Guerrero, R. O. Rodriguez, and R. Torrealba in [Phys. Rev. D **72**, 124012 (2005).]. The values $s = 1$ and $s \geq 3$ correspond to single branes and double branes, respectively. These branes have very rich inner structure. In this paper, by presenting the mass-independent potentials of Kaluza-Klein (KK) modes in the corresponding Schrödinger equations, we investigate the localization and mass spectra of fermions on the symmetric and asymmetric thick branes in an anti-de Sitter background. In order to analyze the effect of gravity-fermion interaction (i.e., the effect of the inner structure of the branes) and scalar-fermion interaction to the spectrum of fermion KK modes, we consider three kinds of typical kink-fermion couplings. The spectra of left chiral fermions for these couplings consist of a bound zero mode and a series of gapless continuous massive KK modes, some discrete bound KK modes including zero mode (exist mass gaps), and a series of continuous massive KK modes, infinite discrete bound KK modes, respectively. The structures of the spectra are investigated in detail.

DOI: 10.1103/PhysRevD.80.065020 PACS numbers: 11.27.+d

I. INTRODUCTION

The suggestion that our observed four-dimensional world is a brane embedded in a higher-dimensional space-time [1–5] can provide new insights for solving gauge hierarchy problem and cosmological constant problem, etc. In the framework of brane scenarios, gravity is free to propagate in all dimensions, while all the matter fields are confined to a 3-brane. By introducing large extra dimensions, the Arkani-Hamed-Dimopoulos-Dvali brane model [3] drops the fundamental Planck scale to Tev. However, it introduces intermediate mass scales corresponding to the large extra dimensions between Planck and Tev scales. In Ref. [4], an alternative scenario, Randall-Sundrum (RS) warped brane model, was proposed. In this scenario, the internal manifold does not need to be compactified to the Planck scale anymore and the exponential warp factor in the metric can generate a large hierarchy of scales, which are reasons why this new brane model has attracted so much attention.

Generalizations and extensions of the RS brane model have been proposed, for example, in Refs. [6–8]. In Ref. [7], the model with extra dimensions composed of a compact hyperbolic manifold is free of usual problems that plague the original Arkani-Hamed-Dimopoulos-Dvali model and shares many common features with the RS model. Recently, the RS model was generalized to higher dimensions for a multiply space-time with negative cosmological constant [8]. In this generalized scenario, the observed hierarchy in the masses of standard model fermions can be explained geometrically without invoking any further hierarchy among the various moduli provided the warping is large in one direction and small in the other.

In the RS warped scenario, however, the modulus, namely, the brane separation, is not stable. Goldberger and Wise showed that it can be stabilized by introducing a scalar field in the bulk [9]. A bulk scalar also provides us with a way of generating the brane as a domain wall (thick brane) in five dimensions. Considering our four-dimensional Universe as an infinitely thin domain wall is an idealization. It is for this reason that an increasing interest has been focused on the study of thick brane scenarios based on gravity coupled to scalars in higher-dimensional space-time [10–19]. A virtue of these models is that the branes can be obtained naturally rather than introduced by hand. In most thick brane scenarios, the scalar field is a standard topological kink interpolating between the minima of a potential with spontaneously broken symmetry. For a comprehensive review on thick brane solutions and related topics please see Ref. [20].

In brane world scenarios, an important problem is the localization of various bulk fields on a brane by a natural mechanism. Especially, the localization of spin half-fermions on thick branes is very interesting. Localizing fermions on branes or defects requires us to introduce other interactions besides gravity. Recently, localization mechanisms on a domain wall for fermions have been extensively analyzed in Ref. [21]. There are some other backgrounds, for example, gauge field [22,23], supergravity [24], and vortex background [25–28], could be considered. Localization of fermions in general space-times has been studied, for example, in [29]. In five dimensions, with the scalar-fermion coupling, there may exist a single bound

[*]liuyx@lzu.edu.cn
[†]Corresponding author.
[‡]fuche08@lzu.edu.cn
[§]lizhao@lzu.edu.cn
[‖]ysduan@lzu.edu.cn

state and a continuous gapless spectrum of massive fermion Kaluza-Klein (KK) states [30–34], while for some other brane models, there exist finite discrete KK states (mass gaps) and a continuous gapless spectrum starting at a positive m^2 [35–37]. In Ref. [38], it was found that fermions can escape into the bulk by tunnelling, and the rate depends on the parameters of the scalar potential. In Ref. [39], the authors obtained trapped discrete massive fermion states on the brane, which in fact are quasibound and have a finite probability of escaping into the bulk.

In Ref. [40], localization and mass spectra of various bulk matter fields including fermions on symmetric and asymmetric de Sitter thick single branes were investigated. It was shown that the massless modes of scalars and vectors are separated by a mass gap from the continuous modes. The asymmetry may increase the number of the bound KK modes of scalars but does not change that of vectors. The localization property of spin $1/2$ fermions is dependent on the coupling of fermions and the background scalar $\eta\bar{\Psi}F(\phi)\Psi$. For the usual Yukawa coupling with $F(\phi(z)) = \phi(z) \sim \arctan(\sinh z)$ (a usual kink which is almost a constant at large z), the fermion zero mode cannot be localized on the branes. For the scalar-fermion coupling with $F(\phi(z))$ a kink likes $\sinh z$, which increases quickly with z, there exist some discrete bound KK modes and a series of continuous ones, and one of the zero modes of left and right fermions is localized on the branes strongly. The asymmetry reduces the number of the bound fermion KK modes.

Fermions on symmetric and asymmetric double branes have been reported in Ref. [41]. These double branes are stable Bogomol'nyi-Prasad-Sommerfeld thick walls with two subwalls located at their edges. It was shown that, for the symmetric brane, the zero modes of fermions coupled to the scalar field through Yukawa interactions and gravitons are not peaked at the center of the brane, but instead a constant between the two sub-branes. However, in the asymmetric scenario, as a consequence of the asymmetry, fermions are localized on one of the subwalls, while the gravitons are localized on another subwall. Hence a large hierarchy between the Planck and the weak scales can be produced.

In Ref. [42], a three-parameter family of asymmetric thick brane solutions in five dimensions (including single branes and double branes) were constructed from a two-parameter family of symmetric ones given in Refs. [43–45]. These branes have very rich inner structure. In this paper, we will investigate the localization problem and the mass spectra of fermions on the symmetric and asymmetric thick branes for three kinds of typical kink-fermion couplings in detail. It will be shown that the localization properties on asymmetric branes are very different from those given in Refs. [40,41]. The mass spectra of fermions are determined by the inner structures of the branes and the scalar-fermion couplings. The paper is organized as follows: In Sec. II, we first give a brief review of the symmetric and asymmetric double thick branes in an anti-de Sitter (AdS) background. Then, in Sec. III, we study localization of spin half-fermions on the thick branes with different types of scalar-fermion interactions by presenting the shapes of the potentials of the corresponding Schrödinger problem. Finally, a brief discussion and conclusion are presented in Sec. IV.

II. REVIEW OF THE SYMMETRIC AND ASYMMETRIC THICK BRANES

Let us consider thick branes arising from a real scalar field ϕ with a scalar potential $V(\phi)$. The action for such a system is given by

$$S = \int d^5x\sqrt{-g}\left[\frac{1}{2\kappa_5^2}R - \frac{1}{2}g^{MN}\partial_M\phi\partial_N\phi - V(\phi)\right], \quad (1)$$

where R is the scalar curvature and $\kappa_5^2 = 8\pi G_5$ with G_5 the five-dimensional Newton constant. Here we set $\kappa_5 = 1$. The line element for a five-dimensional space-time is assumed as

$$ds^2 = e^{2A(z)}(\eta_{\mu\nu}dx^\mu dx^\nu + dz^2), \quad (2)$$

where $e^{2A(z)}$ is the warp factor and z stands for the extra coordinate. The scalar field is considered to be a function of z only, i.e., $\phi = \phi(z)$. In the model, the potential could provide a thick brane realization, and the soliton configuration of the scalar field dynamically generates the domain wall configuration with warped geometry. The field equations generated from the action (1) with the ansatz (2) reduce to the following coupled nonlinear differential equations:

$$\phi'^2 = 3(A'^2 - A''), \quad (3)$$

$$V(\phi) = \tfrac{3}{2}(-3A'^2 - A'')e^{-2A}, \quad (4)$$

$$\frac{dV(\phi)}{d\phi} = (3A'\phi' + \phi'')e^{-2A}, \quad (5)$$

where the prime denotes the derivative with respect to z. Now we consider static double thick branes in an AdS background. A two-parameter family of symmetric double thick branes in five dimensions for the potential

$$V(\phi) = \tfrac{3}{2}\lambda^2\sin^{2-(2/s)}(\phi/\phi_0)\cos^2(\phi/\phi_0) \times [2s - 1 - 4\tan^2(\phi/\phi_0)], \quad (6)$$

was presented and discussed in Refs. [43,44]:

$$e^{2A} = \frac{1}{[1 + (\lambda z)^{2s}]^{1/s}}, \quad (7)$$

$$\phi = \phi_0 \arctan(\lambda z)^s, \quad (8)$$

where $\phi_0 = \sqrt{3(2s-1)}/s$, λ is a positive real constant, and s is a positive odd integer. This solution represents a family of plane symmetric static single ($s = 1$) or double ($s > 1$) domain wall space-times, being asymptotically AdS_5 with a cosmological constant $-6\lambda^2$. Similar solutions can be found in [45].

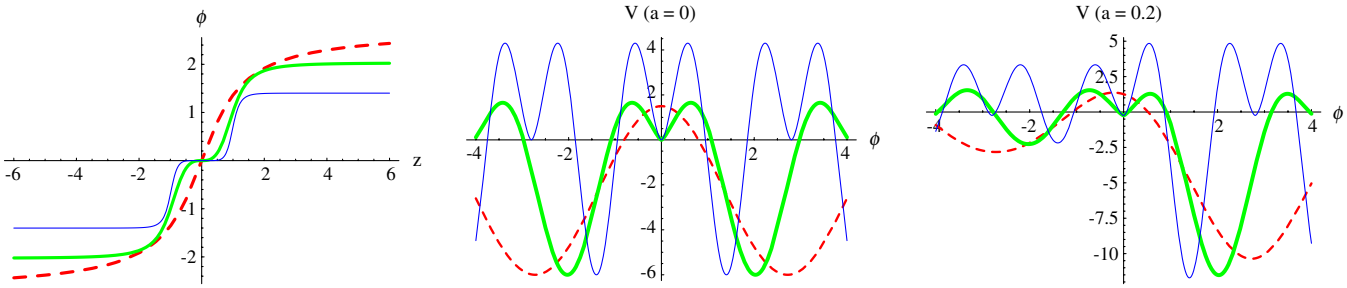

FIG. 1 (color online). The shapes of the kink $\phi(z)$ and the potential $V(\phi)$ for $a = 0$ and 0.2. The parameters are set to $\lambda = 1$, $s = 1$ for the red dashed lines, $s = 3$ for the green thick lines, and $s = 7$ for the blue thin lines.

Based on the symmetric solution above, and in concordance with the approach presented in [42], a three-parameter family of asymmetric thick branes in five dimensions was constructed in Ref. [42]:

$$e^{2A} = \frac{1}{(1 + (\lambda z)^{2s})^{1/s}\mathcal{F}(z)^2}, \tag{9}$$

$$\phi = \phi_0 \arctan(\lambda z)^s, \tag{10}$$

$$\begin{aligned} V(\phi) = & -\tfrac{3}{4}\sin^2(\phi/\phi_0)\tan^{-2/s}(\phi/\phi_0)\mathcal{K}(\phi) \\ & \times \{16a\tan^{1/s}(\phi/\phi_0) + \cos^{-2/s}(\phi/\phi_0) \\ & \times [5 - 2s - (3 + 2s)\cos(2\phi/\phi_0)]\mathcal{K}(\phi)\} \\ & - 6a^2\cos^{2/s}(\phi/\phi_0), \end{aligned} \tag{11}$$

where the asymmetric factor a satisfies

$$0 < a < \frac{\Gamma(1/s)\lambda}{\Gamma(1/2s)\Gamma(1 + 1/2s)}\left(> \frac{\lambda}{2}\right), \tag{12}$$

and $\mathcal{F}(z)$ and $\mathcal{K}(\phi)$ are defined as

$$\mathcal{F}(z) \equiv 1 + az_2F_1\left(\frac{1}{2s}, \frac{1}{s}, 1 + \frac{1}{2s}, -(\lambda z)^{2s}\right), \tag{13}$$

$$\begin{aligned} \mathcal{K}(\phi) \equiv & \lambda + a\tan^{1/s}(\phi/\phi_0)_2F_1 \\ & \times \left(\frac{1}{2s}, \frac{1}{s}, 1 + \frac{1}{2s}, -\tan^2\left(\frac{\phi}{\phi_0}\right)\right). \end{aligned} \tag{14}$$

The parameter a describes the asymmetry of the solution. For $a \to 0$ and $s = 1$ the regularized version of the Randall-Sundrum thin brane will be recovered [11,16]. For $\alpha > 0$ and $s > 1$, this is a solution of an asymmetric static double domain wall space-time interpolating between different AdS_5 vacua. The scalar curvature R and

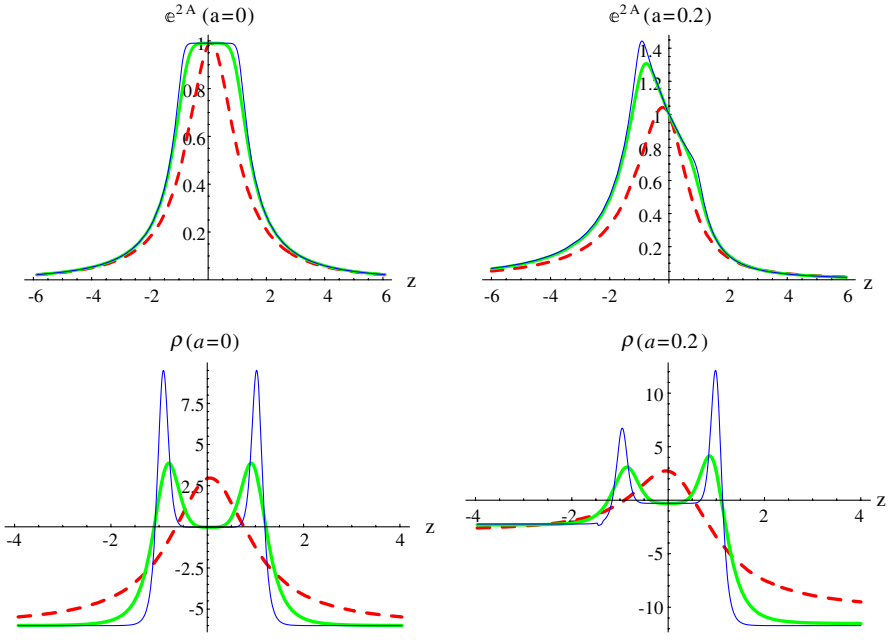

FIG. 2 (color online). The shapes of the warp factor e^{2A} and the energy density ρ for the symmetric ($a = 0$) and asymmetric ($a = 0.2$) thick branes. The parameters are set to $\lambda = 1$, $s = 1$ for the red dashed lines, $s = 3$ for the green thick lines, and $s = 7$ for the blue thin lines.

the energy density ρ for the solution are read

$$R = -\frac{40a(\lambda z)^{2s}}{z(1+(\lambda z)^{2s})}\mathcal{F}(z) - \frac{20a^2}{(1+(\lambda z)^{2s})^{1/s}} - \frac{4(\lambda z)^{2s}(2-4s+5(\lambda z)^{2s})}{z^2(1+(\lambda z)^{2s})^{2-1/s}}\mathcal{F}^2(z), \tag{15}$$

$$\rho = -\frac{12a(\lambda z)^{2s}}{z(1+(\lambda z)^{2s})}\mathcal{F}(z) - \frac{6a^2}{(1+(\lambda z)^{2s})^{1/s}} - \frac{3(\lambda z)^{2s}(1-2s+2(\lambda z)^{2s})}{z^2(1+(\lambda z)^{2s})^{2-1/s}}\mathcal{F}^2(z). \tag{16}$$

The shapes of the kink ϕ, the potential $V(\phi)$, the warp factor e^{2A}, and the energy density ρ are shown in Figs. 1 and 2. It is clear that the single brane is localized at $z=0$, while the two sub-branes are localized at $z=\pm 1/\lambda$ and the thickness of the double brane is $2/\lambda$. When $s\to\infty$, each sub-brane is a thin brane. More detailed discussions can be found in Ref. [42].

III. LOCALIZATION AND MASS SPECTRA OF FERMIONS ON THE THICK BRANES

In this section let us investigate the localization problem of spin 1/2 fermions on the family of symmetric and asymmetric thick branes given in Sec. II by means of the gravitational interaction and scalar-fermion couplings. We will analyze the spectra of fermions on the thick branes by presenting the potential of the corresponding Schrödinger equation. It can be seen from the following calculations that the mass-independent potential can be obtained conveniently with the conformally flat metric (2).

In five dimensions, fermions are four component spinors and their Dirac structure is described by $\Gamma^M = e^M_{\bar{M}}\Gamma^{\bar{M}}$ with $\{\Gamma^M,\Gamma^N\}=2g^{MN}$, where $\bar{M},\bar{N},\cdots=0,1,2,3,5$ denote the five-dimensional local Lorentz indices, and $\Gamma^{\bar{M}}$ are the flat gamma matrices in five dimensions. In our setup, $\Gamma^M=(e^{-A}\gamma^\mu, \mathrm{e}^{-A}\gamma^5)$, where γ^μ and γ^5 are the usual flat gamma matrices in the Dirac representation. The Dirac action of a massless spin 1/2 fermion coupled to the scalar is

$$S_{1/2} = \int d^5x\sqrt{-g}(\bar{\Psi}\Gamma^M D_M\Psi - \eta\bar{\Psi}F(\phi)\Psi), \tag{17}$$

where the covariant derivative D_M is defined as $D_M\Psi = (\partial_M+\omega_M)\Psi$ with the spin connection $\omega_M = \frac{1}{4}\omega_M^{\bar{M}\bar{N}}\Gamma_{\bar{M}}\Gamma_{\bar{N}}$. With the metric (2), the nonvanishing components of the spin connection ω_M are

$$\omega_\mu = \tfrac{1}{2}(\partial_z A)\gamma_\mu\gamma_5. \tag{18}$$

Then the five-dimensional Dirac equation is read as

$$\{\gamma^\mu\partial_\mu + \gamma^5(\partial_z+2\partial_z A) - \eta e^A F(\phi)\}\Psi = 0, \tag{19}$$

where $\gamma^\mu\partial_\mu$ is the Dirac operator on the brane. Note that the sign of the coupling η of the spinor Ψ to the scalar ϕ is arbitrary and represents a coupling either to the kink or antikink domain wall. For definiteness, we shall consider in what follows only the case of a kink coupling, and thus assume that $\eta>0$.

Now we study the above five-dimensional Dirac equation. Because of the Dirac structure of the fifth gamma matrix γ^5, we expect the left- and right-handed projections of the four-dimensional part to behave differently. From the equation of motion (19), we will search for the solutions of the general chiral decomposition

$$\Psi(x,z) = e^{-2A}\sum_n(\psi_{Ln}(x)f_{Ln}(z) + \psi_{Rn}(x)f_{Rn}(z)), \tag{20}$$

where $\psi_{Ln}(x) = -\gamma^5\psi_{Ln}(x)$ and $\psi_{Rn}(x)=\gamma^5\psi_{Rn}(x)$ are the left-handed and right-handed components of a four-dimensional Dirac field, respectively, the sum over n can be both discrete and continuous. Here, we assume that $\psi_L(x)$ and $\psi_R(x)$ satisfy the four-dimensional massive Dirac equations $\gamma^\mu\partial_\mu\psi_{Ln}(x) = m_n\psi_{R_n}(x)$ and $\gamma^\mu\partial_\mu\psi_{Rn}(x) = m_n\psi_{L_n}(x)$. Then $\alpha_L(z)$ and $\alpha_R(z)$ satisfy the following coupled equations:

$$[\partial_z + \eta e^A F(\phi)]f_{Ln}(z) = m_n f_{Rn}(z), \tag{21a}$$

$$[\partial_z - \eta e^A F(\phi)]f_{Rn}(z) = -m_n f_{Ln}(z). \tag{21b}$$

From the above coupled equations, we get the Schrödinger-like equations for the KK modes of the left and right chiral fermions

$$(-\partial_z^2 + V_L(z))f_{Ln} = \mu_n^2 f_{Ln}, \tag{22}$$

$$(-\partial_z^2 + V_R(z))f_{Rn} = \mu_n^2 f_{Rn}, \tag{23}$$

where the effective potentials are given by

$$V_L(z) = (\eta e^A F(\phi))^2 - \partial_z(\eta e^A F(\phi)), \tag{24a}$$

$$V_R(z) = V_L(z)|_{\eta\to-\eta}. \tag{24b}$$

In order to obtain the standard four-dimensional action for the massive chiral fermions

$$\begin{aligned} S_{1/2} &= \int d^5x\sqrt{-g}\bar{\Psi}(\Gamma^M(\partial_M+\omega_M) - \eta F(\phi))\Psi \\ &= \sum_n\int d^4x(\bar{\psi}_{Rn}\gamma^\mu\partial_\mu\psi_{Rn} - \bar{\psi}_{Rn}m_n\psi_{Ln}) \\ &\quad + \sum_n\int d^4x(\bar{\psi}_{Ln}\gamma^\mu\partial_\mu\psi_{Ln} - \bar{\psi}_{Ln}m_n\psi_{Rn}) \\ &= \sum_n\int d^4x\bar{\psi}_n(\gamma^\mu\partial_\mu - m_n)\psi_n, \end{aligned} \tag{25}$$

we need the following orthonormality conditions for f_{L_n} and f_{R_n}:

$$\int_{-\infty}^{\infty} f_{Lm}(z) f_{Ln}(z) dz = \delta_{mn},$$
$$\int_{-\infty}^{\infty} f_{Rm}(z) f_{Rn}(z) dz = \delta_{mn}, \tag{26}$$
$$\int_{-\infty}^{\infty} f_{Lm}(z) f_{Rn}(z) dz = 0.$$

Note that the differential equations (22) and (23) can be factorized as

$$[-\partial_z + \eta e^A F(\phi)][\partial_z + \eta e^A F(\phi)] f_{Ln}(z) = m_n^2 f_{Ln}(z), \tag{27}$$

$$[-\partial_z - \eta e^A F(\phi)][\partial_z - \eta e^A F(\phi)] f_{Rn}(z) = m_n^2 f_{Rn}(z). \tag{28}$$

It can be shown that m_n^2 is zero or positive since the resulting Hamiltonian can be factorized as the product of two operators which are adjoints of each other. Hence the system is stable against linear classical metric and scalar fluctuations.

It can be seen that, in order to localize left or right chiral fermions, there must be some kind of scalar-fermion coupling, and the effective potential $V_L(z)$ or $V_R(z)$ should have a minimum at the location of the brane. Furthermore, for the kink configuration of the scalar $\phi(z)$ (8), $F(\phi(z))$ should be an odd function of $\phi(z)$ when one demands that $V_{L,R}(z)$ are invariant under Z_2 reflection symmetry $z \to -z$. Thus we have $F(\phi(0)) = 0$ and $V_L(0) = -V_R(0) = -\eta \partial_z F(\phi(0))$, which results in the well-known conclusion: only one of the massless left and right chiral fermions could be localized on the brane. The spectra are determined by the behavior of the potentials at infinity. For $V_{L,R} \to 0$ as $|z| \to \infty$, one of the potentials would have a volcanolike shape and there exists only a bound massless mode followed by a continuous gapless spectrum of KK states, while another could not trap any bound states and the spectrum is also continuous and gapless. The simplest Yukawa coupling $F(\phi) = \phi$ and the generalized coupling $F(\phi) = \phi^k$ with positive odd integer $k(\geq 3)$ belong to this type. For $V_{L,R} \to V_\infty =$ constant as $|z| \to \infty$, those modes with $m_n^2 < V_\infty$ belong to discrete spectrum and modes with $m_n^2 > V_\infty$ contribute to a continuous one. For this case, the simplest coupling is of the form $F(\phi) = \tan^{1/s}(\phi/\phi_0)$. If the potentials increase as $|z| \to \infty$, the spectrum is discrete. There are a lot of couplings for the case. The concrete behavior of the potentials is dependent on the function $F(\phi)$. In the following, we will discuss in detail three typical couplings for the above three cases as examples.

A. Case I: $F(\phi) = \phi^k$

We mainly consider the simplest case $F(\phi) = \phi$, for which the explicit forms of the potentials (24) are

$$V_L^S(z) = 3\eta^2 \frac{(2s-1)}{s^2} \frac{\arctan^2(\lambda^s z^s)}{[1+(\lambda z)^{2s}]^{(1/s)}} - \eta \frac{\sqrt{6s-3}}{s} \frac{(\lambda z)^s [s - (\lambda z)^s \arctan(\lambda^s z^s)]}{z[1+(\lambda z)^{2s}]^{1+(1/2s)}}, \tag{29}$$

$$V_R^S(z) = V_L^S(z)|_{\eta \to -\eta}, \tag{30}$$

and

$$V_L^A(z) = \left\{ 3\eta^2 \frac{(2s-1)}{s^2} \frac{\arctan^2(\lambda^s z^s)}{[1+(\lambda z)^{2s}]^{(1/s)}} + a\eta \frac{\sqrt{6s-3}}{s} \frac{\arctan(\lambda^s z^s)}{[1+(z\lambda)^{2s}]^{(3/2s)}} \right\} \frac{1}{\mathcal{F}^2(z)} \tag{31}$$

$$- \eta \frac{\sqrt{6s-3}}{s} \frac{(\lambda z)^s [s - (\lambda z)^s \arctan(\lambda^s z^s)]}{z[1+(\lambda z)^{2s}]^{1+(1/2s)} \mathcal{F}(z)},$$
$$V_R^A(z) = V_L^A(z)|_{\eta \to -\eta}, \tag{32}$$

for the symmetric and asymmetric brane solutions, respectively.

All potentials have the asymptotic behavior: $V_{L,R}^{S,A}(z \to \pm\infty) \to 0$. The values of the potentials for left and right chiral fermions at $z = 0$ are given by

$$V_L^{S,A}(0) = -V_R^{S,A}(0) = \begin{cases} -\sqrt{3}\eta\lambda & \text{for } s = 1. \\ 0 & \text{for } s > 1. \end{cases} \tag{33}$$

So for a given coupling constant η and λ, the values of the potentials for left and right chiral fermions at $z = 0$ are opposite for $s = 1$ and vanish for $s > 1$. Note that there are a single brane and a double brane for $s = 1$ and $s > 1$, respectively. The shapes of the potentials are shown in Fig. 3 for given values of positive η and λ. It can be seen that $V_L(z)$ is indeed a modified volcano type potential for the single brane scenario with $s = 1$, and it has a well. While for the double brane case with $s > 1$, the corresponding potential $V_L(z)$ has a double well, and the potential $V_R(z)$ of right chiral fermions has a single "well," which indicates that there may exist resonances (quasilocalized KK modes). The shape of the potentials is relative to the inner structure of the brane, or equivalently, it depends partly on the warp factor e^{2A}. Furthermore, the coupling type of scalar and fermion also affects the structure of the potentials. For example, for the case $F(\phi) = \phi^k$ with positive odd integer $k \geq 3$, we have $V_{L,R}^{S,A}(0) = 0$ for both $s = 1$ and $s > 1$, and the potentials for left and right chiral fermions have a double well and a single well even for $s = 1$, respectively (see Fig. 4).

Since $V_L^{S,A}(z) \to 0$ when $z \to \pm\infty$, the potentials for left chiral fermions provide no mass gap to separate the fermion zero mode from the excited KK modes. Because the potentials $V_R^{S,A}(z) \geq 0$, there is no bound right chiral fermion zero mode. For both left and right chiral fermions,

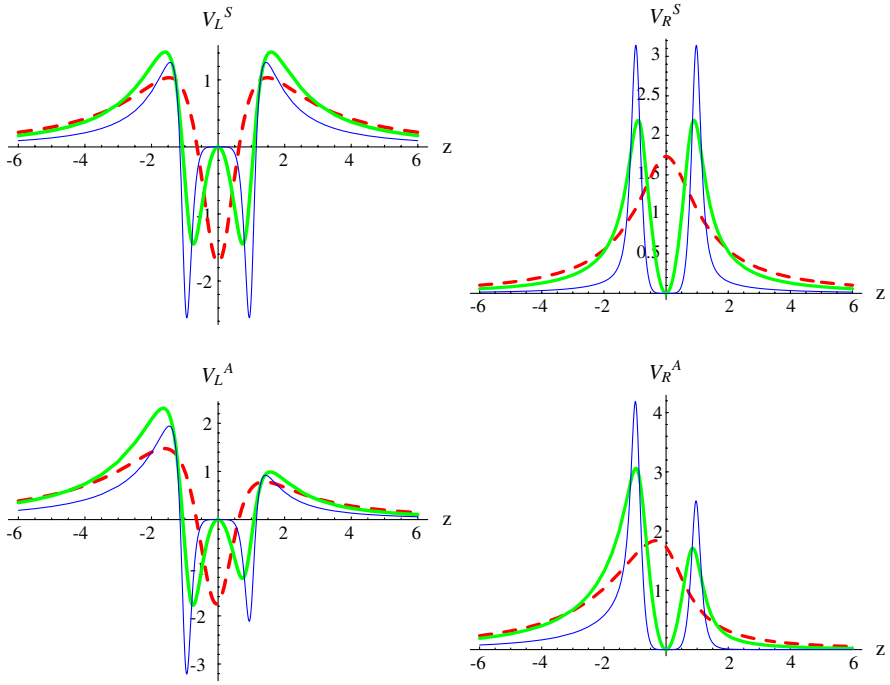

FIG. 3 (color online). The shapes of the symmetric potentials $V^S_{L,R}(a = 0)$ and the asymmetric potentials $V^A_{L,R}(a = 0.2)$ for the left and right chiral fermions for the case $F(\phi) = \phi$. The parameters are set to $\eta = \lambda = 1$ and $s = 1$ for the red dashed lines, $s = 3$ for the green thick lines, and $s = 7$ for the blue thin lines.

there exists a continuous gapless spectrum of the KK modes.

For positive η, only the potentials for left chiral fermions have a negative single well and a double well at the location of the branes for single brane and double brane, respectively, which could trap the left chiral fermion zero mode solved from (21a) by setting $m_0 = 0$:

$$f_{L0}(z) \propto \exp\left(-\eta \int^z d\bar{z} e^{A(\bar{z})} \phi(\bar{z})\right). \tag{34}$$

In order to check the normalization condition (26) for the zero mode (34), we need to check whether the inequality

$$\int f^2_{L0}(z) dz \propto \int \exp\left(-2\eta \int^z d\bar{z} e^{A(\bar{z})} \phi(\bar{z})\right) dz < \infty \tag{35}$$

is satisfied. For the integral $\int dz e^A \phi$, we only need to consider the asymptotic characteristic of the function $\eta e^A \phi$ for $z \to \infty$. For the asymmetric brane scenario, we have

$$2e^A \phi = \frac{2\sqrt{3(2s-1)}\arctan(\lambda z)^s (1 + (\lambda z)^{2s})^{-1/2s}}{s[1 + a z_2 F_1(\frac{1}{2s}, \frac{1}{s}, 1 + \frac{1}{2s}, -(\lambda z)^{2s})]}$$
$$\to \frac{1}{\eta_0 z} \quad \text{for } z \to \infty, \tag{36}$$

where the constant η_0 is given by

$$\eta_0 = \frac{s\lambda}{\sqrt{3(2s-1)}\pi}\left(1 + a\frac{\Gamma(1 + 1/2s)\Gamma(1/2s)}{\lambda\Gamma(1/s)}\right). \tag{37}$$

For the symmetric brane case we only need to take $a = 0$.

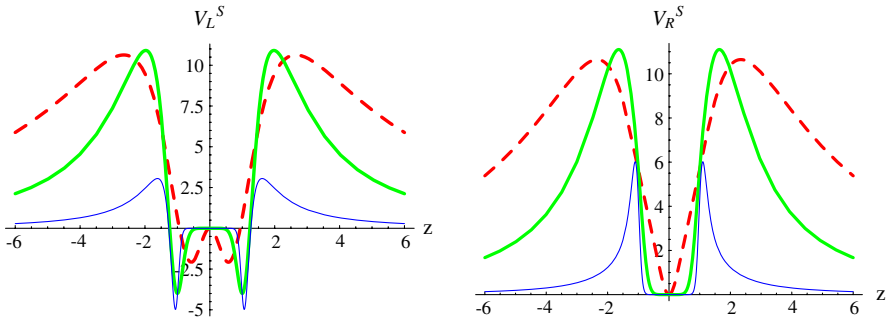

FIG. 4 (color online). The shapes of the potentials $V^S_{L,R}$ for the left and right chiral fermions for the case $F(\phi) = \phi^3$. The parameters are set to $\eta = \lambda = 1$, $s = 1$ for the red dashed lines, $s = 3$ for the green thick lines, and $s = 7$ for the blue thin lines.

So, when $z \to \infty$, we have

$$f_{L0}^2(z) \propto \exp\left(-2\eta \int^z d\bar{z} e^{A(\bar{z})} \phi(\bar{z})\right) \to z^{-\eta/\eta_0}, \quad (38)$$

which indicates that the normalization condition (35) is

$$\eta > \eta_0. \quad (39)$$

Provided the condition (39), the zero mode of left chiral fermions can be localized on the brane. In Refs. [39,46], it was shown that the corresponding zero mode can also be localized on the brane in the background of Sine-Gordon kinks provided a similar condition as (39). While the fermion zero mode cannot be localized on the de Sitter brane with the same coupling $F(\phi) = \phi$ [40]. Note that for large s, η_0 can be approximated as

$$\eta_0 \approx \frac{(\lambda + 2a)}{\sqrt{6}\pi}\sqrt{s}. \quad (40)$$

It is clear that in order for the potentials to localize the zero mode of left chiral fermions for larger s, λ or asymmetric factor a, the stronger coupling of kink and fermions is required. That is to say, the massless mode of the left chiral fermion is easiest to be localized on the symmetric single brane. The asymmetric factor a may destroy the localization of massless fermions. This is different from the situation of the zero modes of scalars and vectors on symmetric and asymmetric de Sitter branes [40], where increasing the asymmetric factor a does not change the number of the bound vector KK modes but would increase that of the bound scalar KK modes, and the zero modes of scalars and vectors are always localized on the de Sitter branes.

In Fig. 5, we plot the left chiral fermion potentials $V_L^{S,A}(z)$ and the corresponding zero modes. We see that the zero modes are bound on the brane. They represents the lowest energy eigenfunction (ground state) of the Schrödinger equation (22) since they have no zeros. Since the ground state has the lowest mass square $m_0^2 = 0$, there is no tachyonic left chiral fermion mode. The zero mode on both the symmetric and asymmetric double walls is essentially constant between the two interfaces. This is very different from the case of gravitons, scalars, and vectors, where the massless modes on the asymmetric double wall are strongly localized only on the interface centered around the lower minimum of the potential. The massive modes will propagate along the extra dimension and those with lower energy would experience an attenuation due to the presence of the potential barriers near the location of the brane.

The potential V_R is always positive near the brane location and vanishes when far away from the brane. This shows that it could not trap any bound fermions with right chirality and there is no zero mode of right chiral fermions. However, the shape of the potential is strongly dependent on the parameter s. For $s \geq 3$, a potential well around the brane location would appear and the well becomes deeper and deeper with the increase of η. The appearance of the potential well could be related to resonances, i.e., massive fermions with a finite lifetime [47,48]. In Ref. [47], a similar potential and resonances for left and

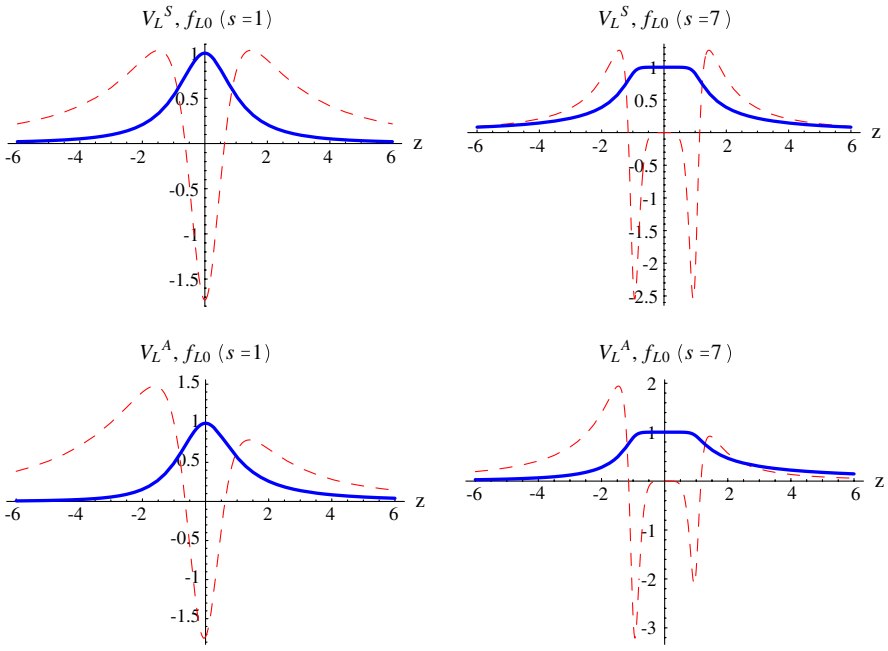

FIG. 5 (color online). The shapes of the zero modes $f_{L0}(z)$ (blue thick lines) and the potentials $V_L^{S,A}(z)$ (red dashing lines) for the symmetric and asymmetric thick branes for the case $F(\phi) = \phi$. The parameters are set to $\eta = \lambda = 1$, $s = 1$ and 7, and $a = 0$ for the above two figures and $a = 0.2$ for the under two figures.

right chiral fermions were found in the background of two-field generated thick branes with internal structure. We can investigate the massive modes of fermions by solving numerically Eqs. (22) and (23).

In Ref. [47], the authors suggested that large peaks in the distribution of $f_{L,R}(0)$ as a function of m would reveal the existence of resonant states. In Ref. [48], we extended this idea and proposed that large relative probabilities for finding massive KK modes within a narrow range $-z_b < z < z_b$ around the brane location, are called $P_{L,R}$, would indicate the existence of resonances. The relative probabilities are defined as follows:

$$P_{L,R}(m) = \frac{\int_{-z_b}^{z_b} |f_{L,R}(z)|^2 dz}{\int_{-z_{\max}}^{z_{\max}} |f_{L,R}(z)|^2 dz}, \tag{41}$$

where we choose $z_b = 0.1 z_{\max}$. For the set of parameters: $\eta = 4$, $\lambda = 1$, and $s = 7$, we find two resonances with mass square 2.4503 and 8.917 for both left and right chiral fermions (see Fig. 6). The configurations of Figs. 6(c) and 6(d) could present the $n = 1$ and $n = 2$ level KK resonance modes of left chiral fermions. The $n = 0$ level mode with left chirality is in fact the only one bound state (the zero mode). While the configurations of Figs. 6(a) and 6(b) present the $n = 0$ and $n = 1$ level resonances of right chiral fermions. We note that the spectra of massive left-handed and right-handed fermionic resonances are the same, which demonstrates that a Dirac fermion could be composed from the left and right resonance KK modes [48]. The lifetime τ for a resonance can be estimated by the width in mass $\Gamma = \Delta m$ at half maximum of the corresponding peak in Fig. 7, which means that the fermion disappears into the extra dimension with time $\tau \sim \Gamma^{-1}$ [49]. The lifetime of the resonances is listed in Table I.

B. Case II: $F(\phi) = \tan^{1/s}(\phi/\phi_0)$

Next, we consider the case $F(\phi) = \tan^{1/s}(\phi/\phi_0)$, for which the potentials take the forms of

$$V_L^S(z) = \frac{\eta^2(\lambda z)^2}{[1+(\lambda z)^{2s}]^{(1/s)}} - \frac{\eta\lambda}{[1+(\lambda z)^{2s}]^{1+(1/2s)}}, \tag{42}$$

$$V_R^S(z) = \frac{\eta^2(\lambda z)^2}{[1+(\lambda z)^{2s}]^{(1/s)}} + \frac{\eta\lambda}{[1+(\lambda z)^{2s}]^{1+(1/2s)}}, \tag{43}$$

and

$$V_L^A(z) = \left\{\frac{\eta^2(\lambda z)^2}{[1+(\lambda z)^{2s}]^{(1/s)}} + \frac{a\eta\lambda z}{[1+(\lambda z)^{2s}]^{(3/2s)}}\right\}\frac{1}{\mathcal{F}^2(z)} - \frac{\eta\lambda}{[1+(\lambda z)^{2s}]^{1+(1/2s)}}\frac{1}{\mathcal{F}(z)}, \tag{44}$$

$$V_R^A(z) = V_L^A(z)|_{\eta\to-\eta}, \tag{45}$$

for the symmetric and asymmetric brane solutions, respectively.

1. The symmetric potential

We first investigate the potential $V_L^S(z)$ (42) for the symmetric brane. It has a minimum (negative value) $-\eta\lambda$ at $z = 0$ and a maximum (positive value) η^2 at $z = \pm\infty$. The shapes of the potential for various parameters are plotted in Fig. 8, from which we can see that they are

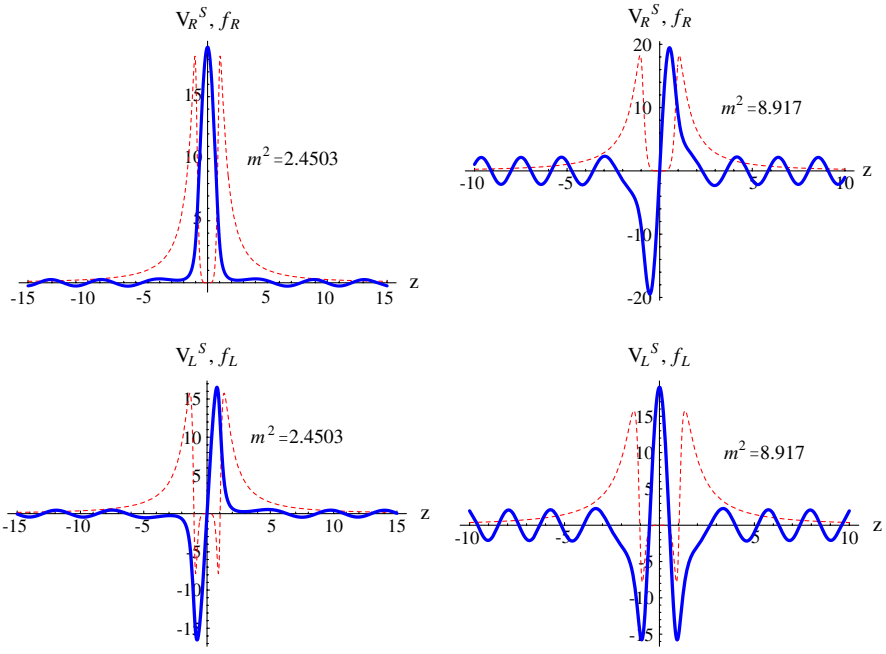

FIG. 6 (color online). The shapes of the fermion resonances (massive modes) $f_{L,R}(z)$ (blue thick lines) and the potentials $V_{L,R}^S(z)$ (red dashing lines) for the symmetric thick branes for the case $F(\phi) = \phi$. The parameters are set to $\eta = 4$, $\lambda = 1$, and $s = 7$.

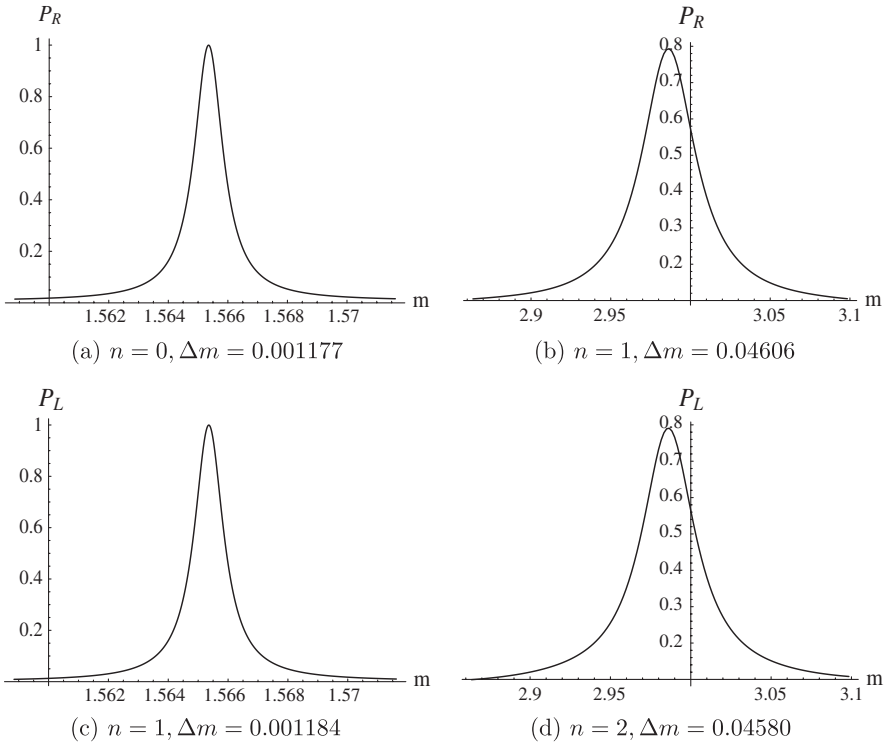

FIG. 7. The probability for finding massive KK modes of the right and left chiral fermions around the brane location, P_R and P_L, as functions of m for the symmetric thick branes for the case $F(\phi) = \phi$. The parameters are set to $\eta = 4$, $\lambda = 1$, and $s = 7$.

similar to that of a Pöschl-Teller (PT) potential for finite s. The massless KK mode can be solved as follows:

$$f_{L0}(z) \propto \exp\left\{-\frac{1}{2}\eta\lambda z^2 {}_2F_1\left(\frac{1}{s}, \frac{1}{2s}, 1+\frac{1}{s}, -(\lambda z)^{2s}\right)\right\}. \quad (46)$$

Because $f_{L0}^2(z) \propto \exp(-2\eta z)$ when $z \to \infty$, the massless KK mode is normalizable without additional conditions, and it would be strongly localized on the brane with large coupling constant η [see Fig. 9(a)]. We note that the potential $V_L^S(z)$ (42) and the zero mode $f_{L0}(z)$ (46) are very different from those given in (29) and (34) for left chiral fermions:

(1) The potential (42) has a single well but the potential (29) has a double well for $s \geq 3$, which results in that the zero mode (46) is strongly localized at the center of the double brane while the zero mode (34) is localized between the two sub-branes of the double brane.

TABLE I. The mass, width, and lifetime for resonances of left and right chiral fermions. The parameters are $\delta = \beta = 0.5$ and $\eta = 10$.

	m^2	m	Γ	τ
$n = 0$ (right)	2.4503	1.5653	0.001 177	849.6
$n = 1$ (left)	2.4503	1.5653	0.001 184	844.5
$n = 1$ (right)	8.9179	2.9863	0.04606	21.71
$n = 2$ (left)	8.9179	2.9863	0.04580	21.83

(2) The potential (42) tends to a positive constant but the potential (29) runs to zero when far away from the brane, which results in that the localization of the zero modes here and (34) is unconditional and conditional [with condition (39)], respectively.

(3) The potential here provides mass gap to separate the zero mode from the excited KK modes.

We have known that the massless KK mode is the lowest state. The massive bound KK modes would appear provided large η. Here we take $\lambda = 1$ for convenience. The number of bound KK modes increases with the coupling constant η. For $\eta = 0.1$, only zero modes are bound for all s. For $\eta = 1$, there are two bound KK modes for $s = 1$ and one bound KK mode (zero mode) for any $s \geq 3$, and the spectra of the KK modes are

$$\begin{aligned} m_{Ln}^2 &= \{0, 0.94\} \cup [1, \infty) \quad \text{for } s = 1, \\ m_{Ln}^2 &= \{0\} \cup [1, \infty) \quad \text{for } s \geq 3. \end{aligned} \quad (47)$$

For $\eta = 6$, there are many bound KK modes for $s = 1$ and four bound KK modes for any $s \geq 3$, and the spectra of the KK modes are

$$\begin{aligned} m_{Ln}^2 &= \{0, 10.59, 18.57, 24.37, 28.44, 31.20, 33.01, 34.17, \\ &\quad 34.89, 35.33, 35.60, 35.76, \cdots\} \cup [36, \infty) \quad \text{for } s = 1, \\ m_{Ln}^2 &= \{0, 11.89, 23.12, 32.21\} \cup [36, \infty) \quad \text{for } s = 3, \\ m_{Ln}^2 &= \{0, 11.99, 23.85, 34.49\} \cup [36, \infty) \quad \text{for } s \to \infty. \end{aligned} \quad (48)$$

The spectra are plotted in Fig. 10. The continuous spectrum

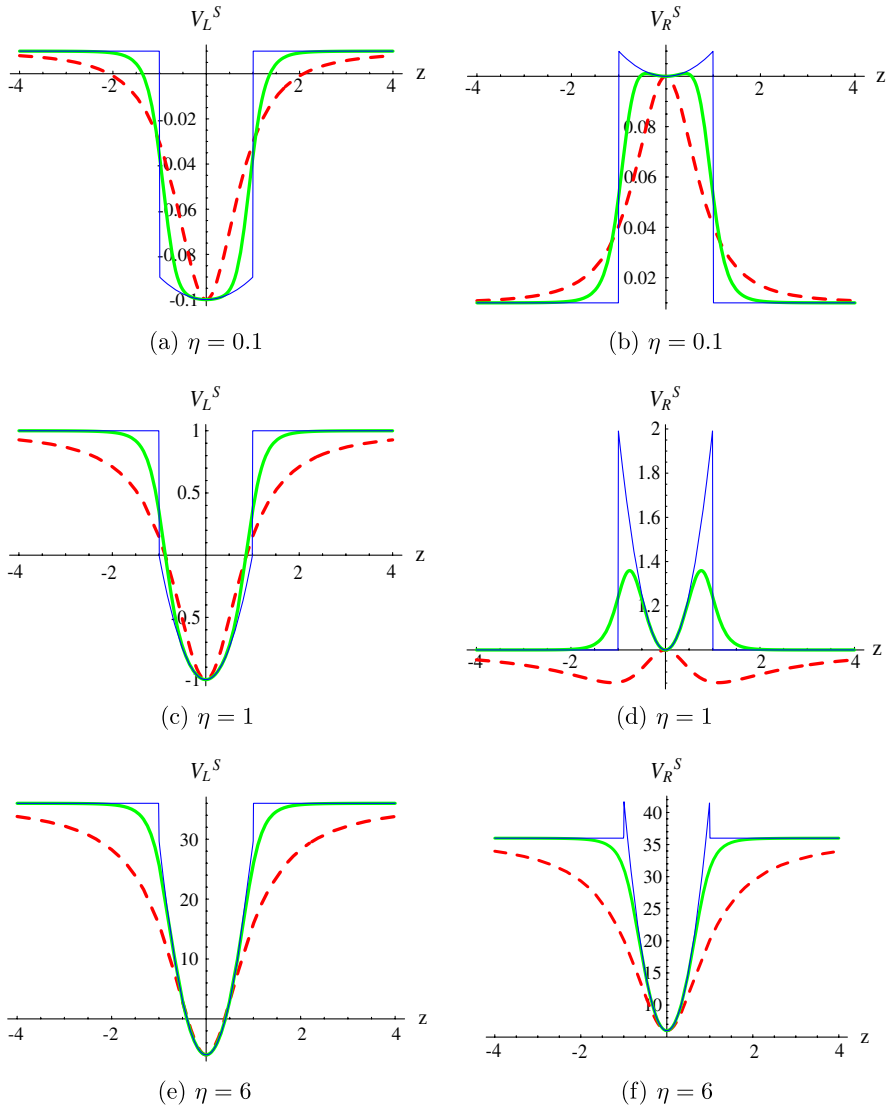

FIG. 8 (color online). The shapes of the potentials $V_L^S(z)$ and $V_R^S(z)$ for the symmetric thick branes for the case $F(\phi) = \tan^{1/s}(\phi/\phi_0)$. The parameter s is set to $s = 1$ for the red dashed lines, $s = 3$ for the green thick lines, and $s \to \infty$ for the blue thin lines. The parameter λ is set to $\lambda = 1$.

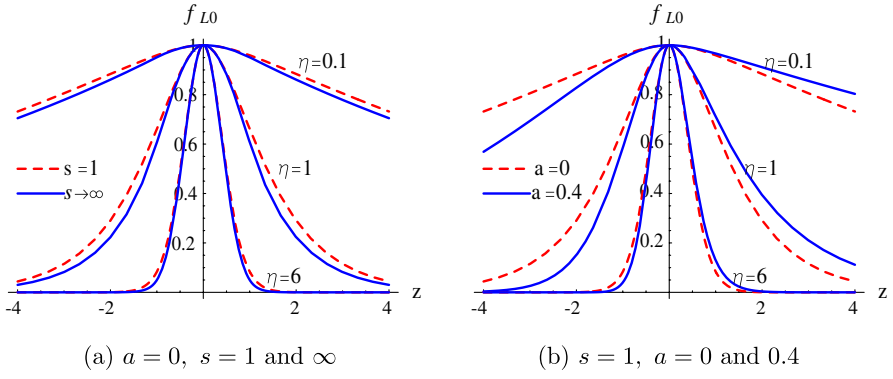

FIG. 9 (color online). The massless modes $f_{L0}(z)$ of the left chiral fermions for the symmetric and asymmetric thick branes for the case $F(\phi) = \tan^{1/s}(\phi/\phi_0)$. The parameters are set to $\lambda = 1$, $\eta = 0.1$, 1, and 6.

starts at $m^2 = \eta^2$ and the KK modes asymptotically turn into plane waves when far away from the brane, which represent delocalized massive KK modes of fermions. It can be seen that the spectrum structure for the single brane scenario with $s = 1$ is very different from that of the double brane scenario with $s \geq 3$. The single brane could trap more massive KK modes than the double brane. Noting that

$$V_L^S(z) = -\eta\lambda + \eta^2(\lambda z)^2 + \frac{2s+1}{2s}\eta\lambda(\lambda z)^{2s} + \mathcal{O}((\lambda z)^{2s+2}),$$

we have the following simple potential for double thin brane scenario ($s \to \infty$):

$$V_L^S(z) = \begin{cases} -\eta\lambda + \eta^2(\lambda z)^2, & |\lambda z| < 1 \\ \eta^2, & |\lambda z| > 1 \end{cases} \quad (49)$$

which could be called "the harmonic oscillator potential well with finite depth." Similar to the square potential well with finite depth, the spectrum can be solved and there are a finite number of bound KK modes.

The shape of the symmetric potential $V_R^S(z)$ (43) for right chiral fermions is more complex than that of left chiral fermions. It has a positive value $\eta\lambda$ at $z = 0$ and trends to η^2 at $z = \pm\infty$. The shapes of the potential for various parameters are plotted in Fig. 8. For small η, the potential for any s has no well to trap bound KK modes. With the increase of η, the potential for $s \geq 3$ will appear a single well, while the potential for $s = 1$ will first appear a double well and then become a single well. For large η, they are similar to a PT potential only for small s [see Fig. 8(f)]. The massless KK mode for right chiral fermions is absent. The number of bound KK modes increases with the coupling constant η. For $\eta = 0.1$, there is no bound KK mode for all s. For $\eta = 1$, there is one bound KK mode for $s = 1$ and no bound KK mode for any $s \geq 3$, and the spectra of the KK modes are

$$\begin{aligned} m_{Rn}^2 &= \{0.94\} \cup [1, \infty) \quad \text{for } s = 1, \\ m_{Rn}^2 &= \{\} \cup [1, \infty) \quad \text{for } s \geq 3. \end{aligned} \quad (50)$$

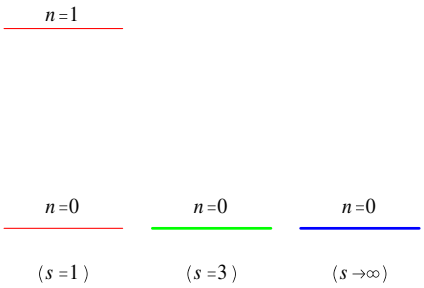

(a) $\eta = 1$

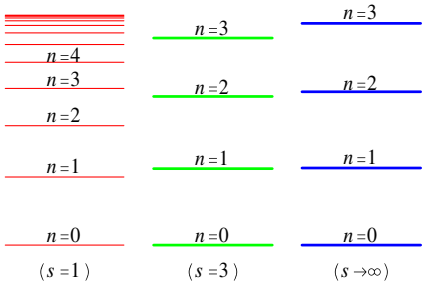

(b) $\eta = 6$

FIG. 10 (color online). The spectra m_{Ln}^2 of bound KK modes of the left chiral fermions for the symmetric thick branes with $F(\phi) = \tan^{1/s}(\phi/\phi_0)$. The parameters are set to $\lambda = 1$, $\eta = 1$ and 6, $s = 1$, 3, and $s \to \infty$.

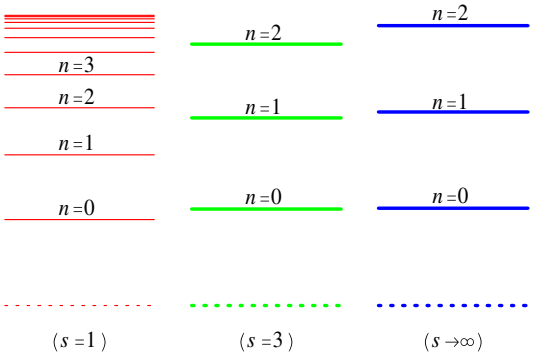

FIG. 11 (color online). The spectra m_{Rn}^2 of bound KK modes of right chiral fermions for the symmetric thick branes for the case $F(\phi) = \tan^{1/s}(\phi/\phi_0)$ with $s = 1$, 3, and $s \to \infty$. The parameters are set to $\lambda = 1$ and $\eta = 6$. The dashed lines denote the absence of the zero modes.

For $\eta = 6$, there are many bound KK modes for $s = 1$ and three bound KK modes for any $s \geq 3$:

$$\begin{aligned} m_{Rn}^2 &= \{10.59, 18.57, 24.37, 28.44, 31.20, 33.01, 34.17, \\ &\quad 34.89, 35.33, 35.60, 35.76, \cdots\} \cup [36, \infty) \quad \text{for } s = 1, \\ m_{Rn}^2 &= \{11.89, 23.12, 32.21\} \cup [36, \infty) \quad \text{for } s = 3, \\ m_{Rn}^2 &= \{11.99, 23.85, 34.49\} \cup [36, \infty) \quad \text{for } s \to \infty. \end{aligned} \quad (51)$$

The spectra are plotted in Fig. 11. The continuous spectrum starts also at $m^2 = \eta^2$. It can be seen that the single brane could also trap more massive KK modes than the double brane. By comparing the mass spectra of right chiral fermions (50) and (51) with the ones of left chiral fermions (47) and (48) for $\eta = 1$ and $\eta = 6$, respectively, we come to the conclusion that the number of bound states of right chiral fermions N_R is one less than that of left ones N_L, i.e., $N_R = N_L - 1$. The mass spectra are almost the same, and the only one difference is the absence of the zero mode of right chiral fermions. Although a potential well around the brane location appears for $s \geq 3$ in Fig. 8(d), we do not find any resonance.

2. The asymmetric potential

Next, let us turn to the potentials (44) and (45) for the asymmetric brane. We note that, because of the appearance of the asymmetric factor a, the potentials have different limits at $z = \pm\infty$:

$$V^A_{L,R}(+\infty) = \frac{\eta^2}{(1 + a\frac{\Gamma(1/2s)\Gamma(1+1/2s)}{\lambda\Gamma(1/s)})^2}, \tag{52}$$

$$V^A_{L,R}(-\infty) = \frac{\eta^2}{(1 - a\frac{\Gamma(1/2s)\Gamma(1+1/2s)}{\lambda\Gamma(1/s)})^2}. \tag{53}$$

For $s = 1$ and $s \to \infty$, we have

$$V^A_{L,R}(\pm\infty) = \frac{\eta^2}{(1 \pm \frac{\pi}{2}\frac{a}{\lambda})^2} \tag{54}$$

and

$$V^A_{L,R}(\pm\infty) \to \frac{\eta^2}{(1 \pm 2\frac{a}{\lambda})^2}, \tag{55}$$

respectively. The constrain condition (12), i.e., $0 < a\frac{\Gamma(1/2s)\Gamma(1+1/2s)}{\lambda\Gamma(1/s)} < 1$, implies

$$0 < \frac{\eta^2}{4} < V^A_{L,R}(\infty) < \eta^2 < V^A_{L,R}(-\infty) < \infty. \tag{56}$$

Hence, comparing with the symmetric potentials $V^S_{L,R}(z)$ (42) and (43), the value of the asymmetric potentials $V^A_{L,R}(z)$ (44) and (45) are enlarged at $z \to +\infty$ and diminished at $z \to -\infty$, which would reduce the number of the bound KK modes of left and right fermions. The shapes of the potentials for various parameters are plotted in Figs. 12 and 13.

The massless KK mode of left chiral fermions

$$f_{L0}(z) \propto \exp\left(\int^z d\bar{z}\frac{-\eta\lambda\bar{z}[1 + (\lambda\bar{z})^{2s}]^{-(1/2s)}}{1 + a\bar{z}_2F_1(\frac{1}{2s}, \frac{1}{s}, 1 + \frac{1}{2s}, -(\lambda\bar{z})^{2s})}\right) \tag{57}$$

is also normalizable, and can be localized on the brane without additional conditions. The effect of the asymmetric factor a and the coupling constant η to the zero mode is shown in Fig. 9(b). It can be seen that, with the increase of η, the effect of the asymmetric factor a can be neglected. However, the effect of a to the number of bound KK modes is remarkable. We also take $\lambda = 1$ here. For $\eta = 0.1$, only zero modes of left chiral fermions are bound for all s and a. For $\eta = 1$ and very small a, there is one bound massive KK mode of both the right and left chiral fermions for $s = 1$, and no bound massive KK mode for $s \geq 3$. For $\eta = 1$ and large a, only massless modes of left chiral fermions are bound for all s. For $\eta = 6$ and $a = 0.2$, there are only three and two bound KK modes of left chiral fermions for $s = 1$ and $s \geq 3$, respectively, and the spectra of the KK modes are

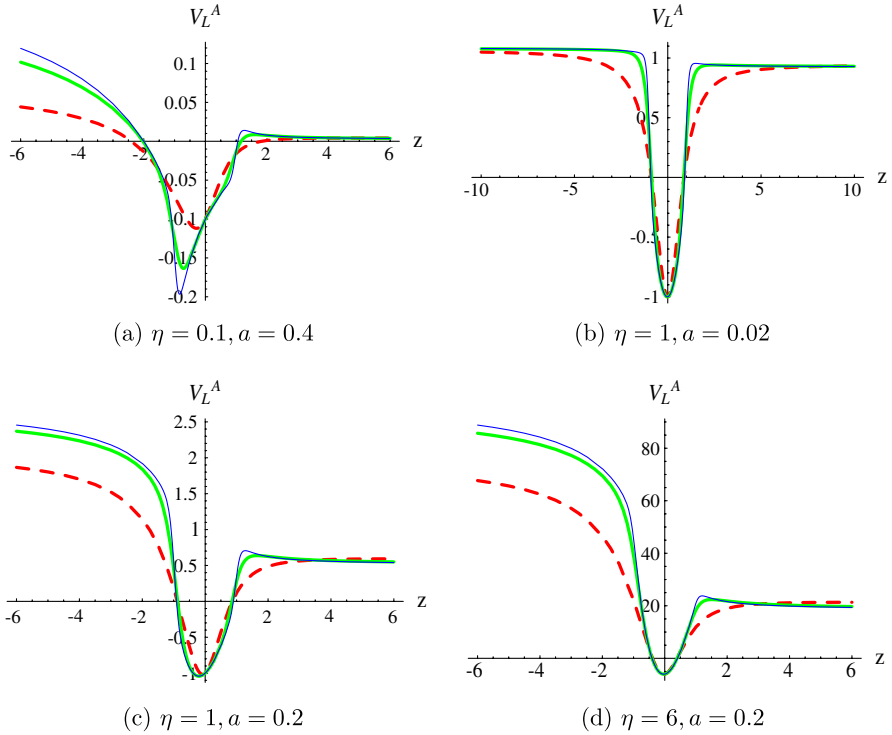

(a) $\eta = 0.1, a = 0.4$ (b) $\eta = 1, a = 0.02$

(c) $\eta = 1, a = 0.2$ (d) $\eta = 6, a = 0.2$

FIG. 12 (color online). The shapes of the asymmetric potential $V^A_L(z)$ for the case $F(\phi) = \tan^{1/s}(\phi/\phi_0)$. The parameter s is set to $s = 1$ for the red dashed lines, $s = 3$ for the green thick lines, and $s = 7$ for the blue thin lines. The parameter λ is set to $\lambda = 1$.

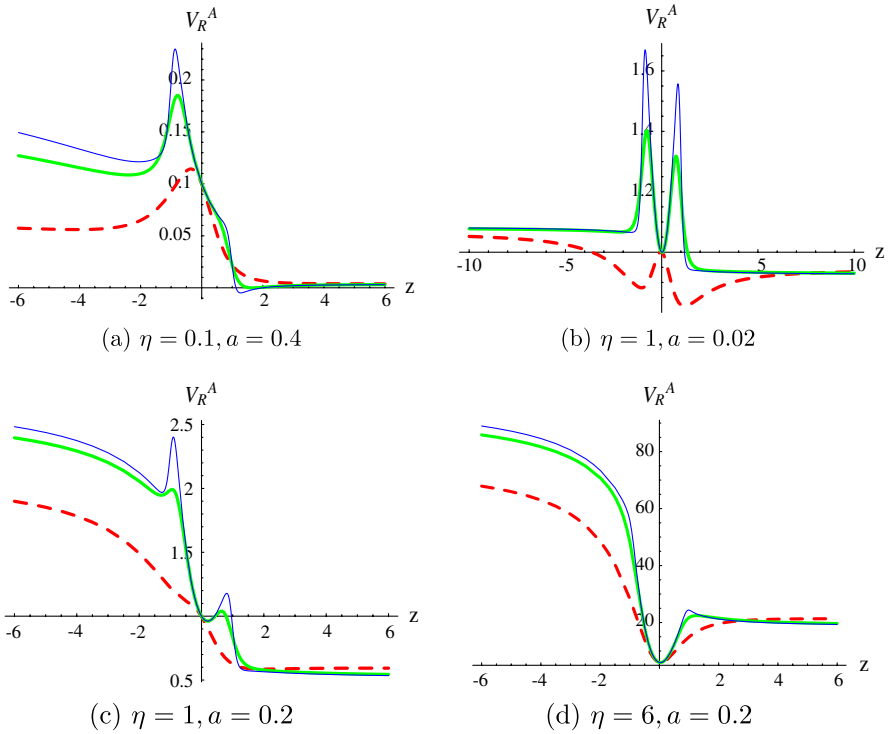

FIG. 13 (color online). The shapes of the asymmetric potential $V_R^A(z)$ for the case $F(\phi) = \tan^{1/s}(\phi/\phi_0)$. The parameters are the same as Fig. 11.

$$
\begin{aligned}
m_{Ln}^2 &= \{0, 10.40, 17.42\} \cup [20.85, \infty) \quad \text{for } s = 1, \\
m_{Ln}^2 &= \{0, 11.74\} \cup [18.75, \infty) \quad \text{for } s = 3, \\
m_{Ln}^2 &= \{0, 11.77\} \cup [18.37, \infty) \quad \text{for } s \to \infty,
\end{aligned} \tag{58}
$$

and

$$
\begin{aligned}
m_{Rn}^2 &= \{10.40, 17.42\} \cup [20.85, \infty) \quad \text{for } s = 1, \\
m_{Rn}^2 &= \{11.74\} \cup [18.75, \infty) \quad \text{for } s = 3, \\
m_{Rn}^2 &= \{11.77\} \cup [18.37, \infty) \quad \text{for } s \to \infty,
\end{aligned} \tag{59}
$$

for left and right chiral fermions, respectively. The spectra for left chiral fermions are shown in Fig. 14. The continuous spectrum starts at different values for different s. It can be seen that the spectrum structure for the single brane case with $s = 1$ is dramatically changed by the asymmetric factor a, i.e., the number of bound KK modes quickly decreases with the increase of a.

C. Case III: $F(\phi) = \tan^{k/s}(\phi/\phi_0)$

For the case $F(\phi) = \tan^{k/s}(\phi/\phi_0)$, considering the expression of ϕ (8), we have $F(\phi(z)) = (\lambda z)^k$. The potential (24a) for the asymmetric brane solution reads as

$$
\begin{aligned}
V_L^A(z) = &\left\{\frac{\eta^2(\lambda z)^{2k}}{[1 + (\lambda z)^{2s}]^{1/s}} + \frac{\eta a(\lambda z)^k}{[1 + (\lambda z)^{2s}]^{3/2s}}\right\}\frac{1}{\mathcal{F}^2(z)} \\
&- \frac{\eta\lambda(\lambda z)^{k-1}[k + (k-1)(\lambda z)^{2s}]}{[1 + (\lambda z)^{2s}]^{1+1/2s}}\frac{1}{\mathcal{F}(z)}.
\end{aligned} \tag{60}
$$

The special value $k = 1$ belongs to case II considered in Subsec. III B. Taking $a = 0$, we will get the potential of left chiral fermions for the symmetric brane solution:

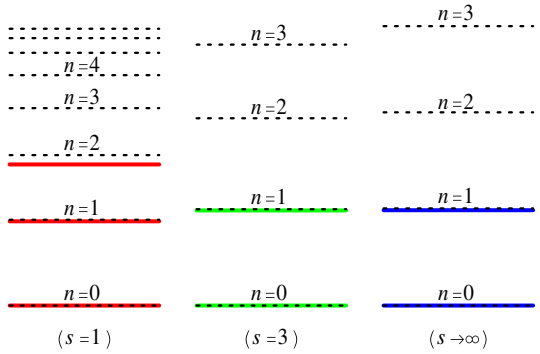

FIG. 14 (color online). The spectra m_{Ln}^2 (solid lines) of bound KK modes of the left chiral fermions for the asymmetric thick branes for the case $F(\phi) = \tan^{1/s}(\phi/\phi_0)$. The parameters are set to $a = 0.2$, $\lambda = 1$, $\eta = 6$, $s = 1, 3$, and $s \to \infty$. The dashing lines denote the corresponding spectra with $a = 0$.

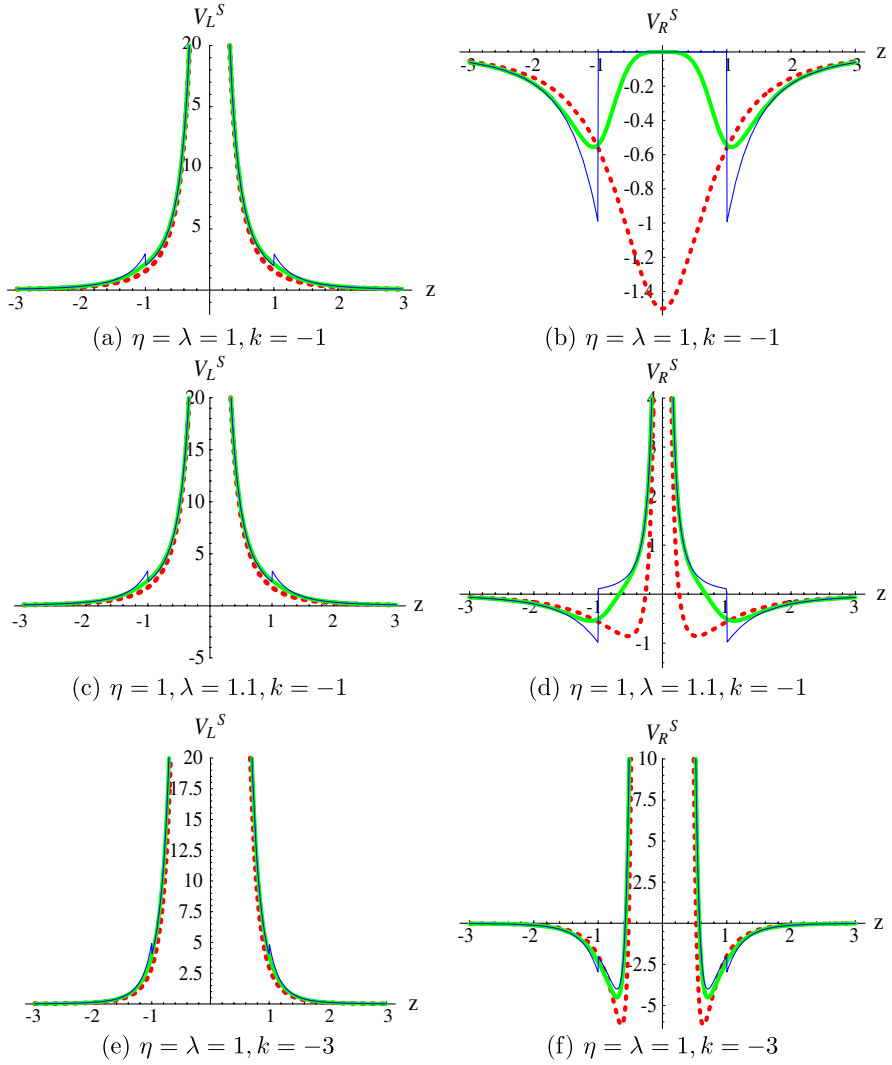

FIG. 15 (color online). The shapes of the symmetric potentials $V_L^S(z)$ and $V_R^S(z)$ for the case $F(\phi) = \tan^{k/s}(\phi/\phi_0)$ with odd $k < 0$. The parameter s is set to $s = 1$ for the red dashed lines, $s = 3$ for the green thick lines, and $s \to \infty$ for the blue thin lines.

$$V_{L,R}^S(z) = \frac{\eta^2(\lambda z)^{2k}}{[1+(\lambda z)^{2s}]^{1/s}} \mp \frac{\eta\lambda(\lambda z)^{k-1}[k+(k-1)(\lambda z)^{2s}]}{[1+(\lambda z)^{2s}]^{1+/1/2s}}. \tag{61}$$

1. The symmetric potential

Let us first analyze the asymptotic property of the symmetric potential. When $z \to \infty$, $1 + (\lambda z)^{2s} \to (\lambda z)^{2s}$, we have

$$\begin{aligned} V_{L,R}^S(z \to \infty) &\to \eta^2(\lambda z)^{2k-2} \mp \eta\lambda k(\lambda z)^{k-2-2s} \\ &\quad \mp \eta\lambda(k-1)(\lambda z)^{k-2} \\ &\to \begin{cases} \eta^2(\lambda z)^{2k-2} \to \infty & \text{for } k > 1 \\ \eta^2 > 0 & \text{for } k = 1 \\ 0 & \text{for } k < 1 \end{cases}. \end{aligned} \tag{62}$$

When $z \to 0$, $1 + (\lambda z)^{2s} \to 1$, we have

$$\begin{aligned} V_{L,R}^S(z \to 0) &\to \eta^2(\lambda z)^{2k}\left(1 - \frac{1}{s}(\lambda z)^{2s}\right) \\ &\quad \mp \eta\lambda(\lambda z)^{k-1}[k+(k-1)(\lambda z)^{2s}] \\ &\quad \times \left(1 - \frac{2s+1}{2s}(\lambda z)^{2s}\right) \\ &\to \begin{cases} 0 & \text{for } k > 1 \\ \mp\eta\lambda & \text{for } k = 1 \\ \frac{\eta(\eta\pm\lambda)}{(\lambda z)^2} + (-\eta^2 \pm \frac{1}{2}\eta\lambda)\delta_{s,1} & \text{for } k = -1 \\ \infty & \text{for } k < -1 \end{cases}. \end{aligned} \tag{63}$$

For $\eta > 0$, $\lambda > 0$, and $k = -1$,

$$V_L^S(z \to 0) \to \infty \tag{64}$$

$$V_R^S(z \to 0) \to \begin{cases} \infty & \text{for } \eta \neq \lambda \\ -\frac{3}{2}\eta^2 & \text{for } \eta = \lambda, s = 1. \\ 0 & \text{for } \eta = \lambda, s > 1 \end{cases} \quad (65)$$

The shapes of the symmetric potentials $V_L^S(z)$ and $V_R^S(z)$ for the case $F(\phi) = \tan^{k/s}(\phi/\phi_0)$ with odd $k < 0$ and $k > 1$ are plotted in Figs. 15 and 16, respectively. For the case $k < 0$, the symmetric potential $V_L^S(z)$ of left chiral fermions has no well and cannot trap any bound KK modes. For right chiral fermions, the symmetric potential $V_R^S(z)$ with $k < -1$ or $k = -1$, $\eta \neq \lambda$, has a double well and a infinite high bar, which can also not trap the massless mode. However, the case $k = -1$, $\eta = \lambda > 0$ is very special, for which $V_R^S(z)$ has a single well (for $s = 1$) or a double well (for $s \geq 3$) [see Fig. 15(b)]. The bound KK modes corresponding to the potentials shown in Fig. 15(b) for $s = 1$, $s = 3$, and $s \to \infty$ have mass square -0.636, -0.1485, and -0.119, respectively. Because all the potentials with $k < 0$ cannot trap zero modes, or even more, some of them could result in tachyonic KK modes with $m^2 < 0$, we do not consider the corresponding kink-fermion coupling of the type $\eta\bar{\Psi}\tan^{k/s}(\phi/\phi_0)\Psi$ with $k < 0$.

For $k > 1$, which is the case we are interested in here, the potentials $V_{L,R}^S(z)$ trend to infinite when far away from the brane and vanish at $z = 0$, which shows that there exist infinite discrete bound KK modes. We note from Fig. 16 that the influence of s is not important. For examples, the spectra for $k = 3$ and $k = 11$ are calculated as

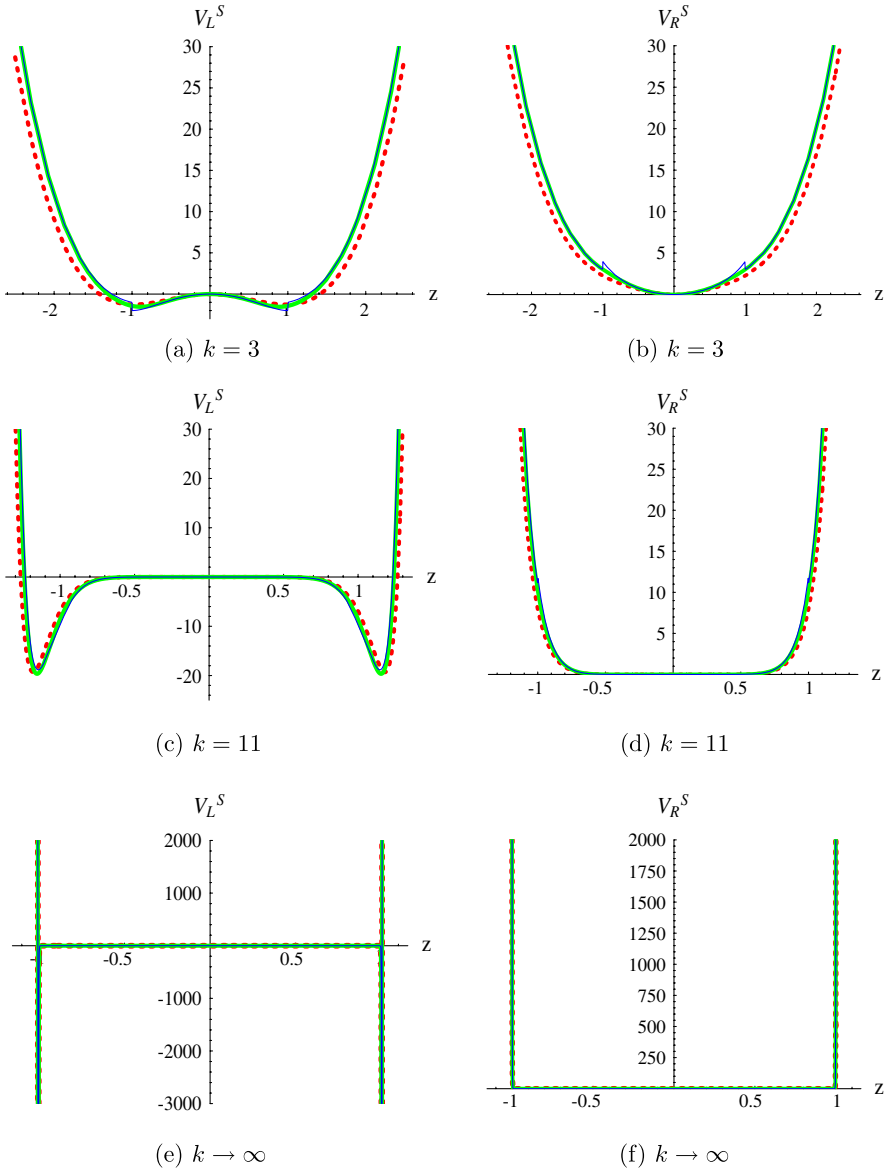

FIG. 16 (color online). The shapes of the symmetric potentials $V_L^S(z)$ and $V_R^S(z)$ for the case $F(\phi) = \tan^{k/s}(\phi/\phi_0)$ with odd $k \geq 3$. The parameter s is set to $s = 1$ for the red dashed lines, $s = 3$ for the green thick lines, and $s \to \infty$ for the blue thin lines. The other parameters are set to $\eta = \lambda = 1$ and $k = 3, 11, \infty$.

$$\begin{aligned} m_{Ln}^2 &= \{0, 1.57, 4.80, 8.44, 12.61, 17.17, 22.08, 27.30, 32.78, 38.52, 44.49, \cdots\} \quad \text{for } s = 1, \\ m_{Ln}^2 &= \{0, 1.76, 5.39, 9.33, 13.73, 18.56, 23.70, 29.14, 34.85, 40.80, 46.97, \cdots\} \quad \text{for } s = 3, \\ m_{Ln}^2 &= \{0, 1.81, 5.52, 9.44, 13.77, 18.65, 23.81, 29.19, 34.93, 40.88, 47.02, \cdots\} \quad \text{for } s \to \infty, \end{aligned} \tag{66}$$

and

$$\begin{aligned} m_{Ln}^2 &= \{0, 1.86, 7.30, 16.02, 27.68, 42.03, 58.93, 78.30, 100.08, 124.22, \cdots\} \quad \text{for } s = 1, \\ m_{Ln}^2 &= \{0, 1.93, 7.59, 16.66, 28.77, 43.67, 61.21, 81.30, 103.87, 128.88, \cdots\} \quad \text{for } s = 3, \\ m_{Ln}^2 &= \{0, 1.96, 7.69, 16.87, 29.12, 44.15, 61.81, 82.00, 104.68, 129.82, \cdots\} \quad \text{for } s \to \infty, \end{aligned} \tag{67}$$

respectively, and shown in Fig. 17.

With the increase of k, the potentials vanish in a more wide range around $z = 0$. Especially, for $k \to \infty$, we get an infinite deep square well for right-hand fermions:

$$V_R^S = \begin{cases} \infty, & |z| > 1/\lambda \\ 0, & |z| < 1/\lambda \end{cases}. \tag{68}$$

The KK modes and the spectrum reads as

$$f_{Rn} = \begin{cases} \sqrt{\lambda}\cos(n\pi\lambda z/2), & n = 1, 3, 5, \cdots \\ \sqrt{\lambda}\sin(n\pi\lambda z/2), & n = 2, 4, 6, \cdots \end{cases} \tag{69}$$

$$m_{Rn}^2 = \left(\frac{\pi}{2}\lambda n\right)^2 (n = 1, 2, 3, \cdots) \tag{70}$$

The numeric result for $k = 13\,111$, $s = \eta = \lambda = 1$ is

$$m_{Rn}^2 = \{2.46, 9.85, 22.16, 39.39, 61.54, 88.62, \cdots\}, \tag{71}$$

from which we have

$$\frac{m_{Rn}}{m_{R1}} = \{1, 2.001, 3.001, 4.002, 5.002, 6.002, \cdots\}. \tag{72}$$

For left-hand fermions, the spectrum also takes the form (70) but with $n = 0, 1, 2, \cdots$, the KK modes can be calculated from Eqs. (21b) and (69) as

$$f_{Ln} = \begin{cases} -\sqrt{\lambda}\sin(n\pi\lambda z/2), & n = 1, 3, 5, \cdots \\ \begin{cases} \lambda/2, & |z| < 1/\lambda \\ 0, & |z| > 1/\lambda \end{cases}, & n = 0 \\ -\sqrt{\lambda}\cos(n\pi\lambda z/2), & n = 2, 4, 6, \cdots \end{cases}. \tag{73}$$

The comparing of spectra of left chiral fermions for different k is shown in Fig. 18.

2. Asymmetric branes

At last, we consider the asymmetric potential (60) for left chiral fermions and the corresponding asymmetric potential (24b) for right chiral fermions. The asymptotic property is analyzed as follows. When $z \to \pm\infty$, $1 + (\lambda z)^{2s} \to (\lambda z)^{2s}$, $\mathcal{F}(z) \to (1 \pm a\frac{\Gamma(1/2s)\Gamma(1+1/2s)}{\lambda\Gamma(1/s)})$, we have

$$V_{L,R}^A(z) \to \begin{cases} \frac{\eta^2(\lambda z)^{2k-2}}{(1\pm a\frac{\Gamma(1/2s)\Gamma(1+1/2s)}{\lambda\Gamma(1/s)})^2} \to \infty & \text{for } k > 1 \\ \frac{\eta^2}{(1\pm a\frac{\Gamma(1/2s)\Gamma(1+1/2s)}{\lambda\Gamma(1/s)})^2} > 0 & \text{for } k = 1 \\ 0 & \text{for } k < 1 \end{cases}. \tag{74}$$

Since $V_{L,R}^S(z \to \pm\infty)$ are finite for $k \le 3$, we only consider the case $k \ge 3$ here, for which $V_{L,R}^S(z \to 0) \to 0$. Comparison of the asymmetric potential $V_L^A(z)$ with the symmetric one $V_L^S(z)$ for the case $F(\phi) = \tan^{k/s}(\phi/\phi_0)$ with different k and s is shown in Fig. 19. We see that, for a fixed finite k, the difference of the two potentials would become large with the increase of s. For $s \to \infty$, the difference is largest. While for a fixed s, the difference of the two potentials would become small with the increase of k. The spectra for $k = 3$ and $k = 11$ are calculated as

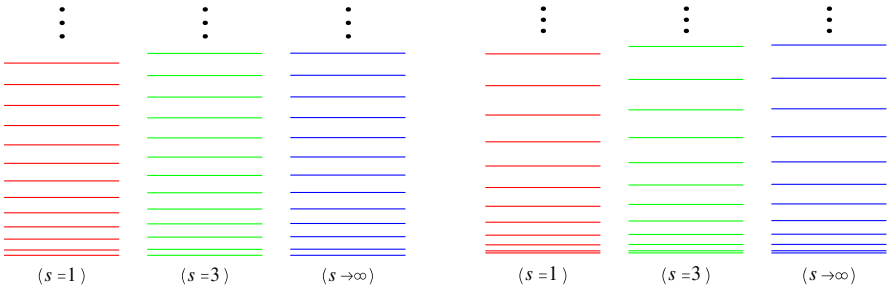

(a) $k = 3$ (b) $k = 11$

FIG. 17 (color online). The spectra m_{Ln}^2 of the left chiral fermions for the case $F(\phi) = \tan^{k/s}(\phi/\phi_0)$ with $k = 3$ and 11. The parameters are set to $a = 0$, $\eta = \lambda = 1$, $s = 1$, 3, and ∞.

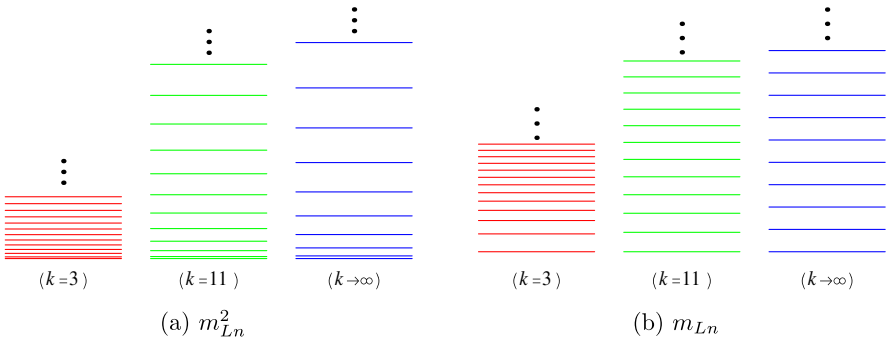

(a) m_{Ln}^2 (b) m_{Ln}

FIG. 18 (color online). The spectra m_{Ln}^2 and m_{Ln} of the left chiral fermions for the case $F(\phi) = \tan^{k/s}(\phi/\phi_0)$ with $k = 3$, 11, and ∞. The parameters are set to $a = 0$, $s = \eta = \lambda = 1$.

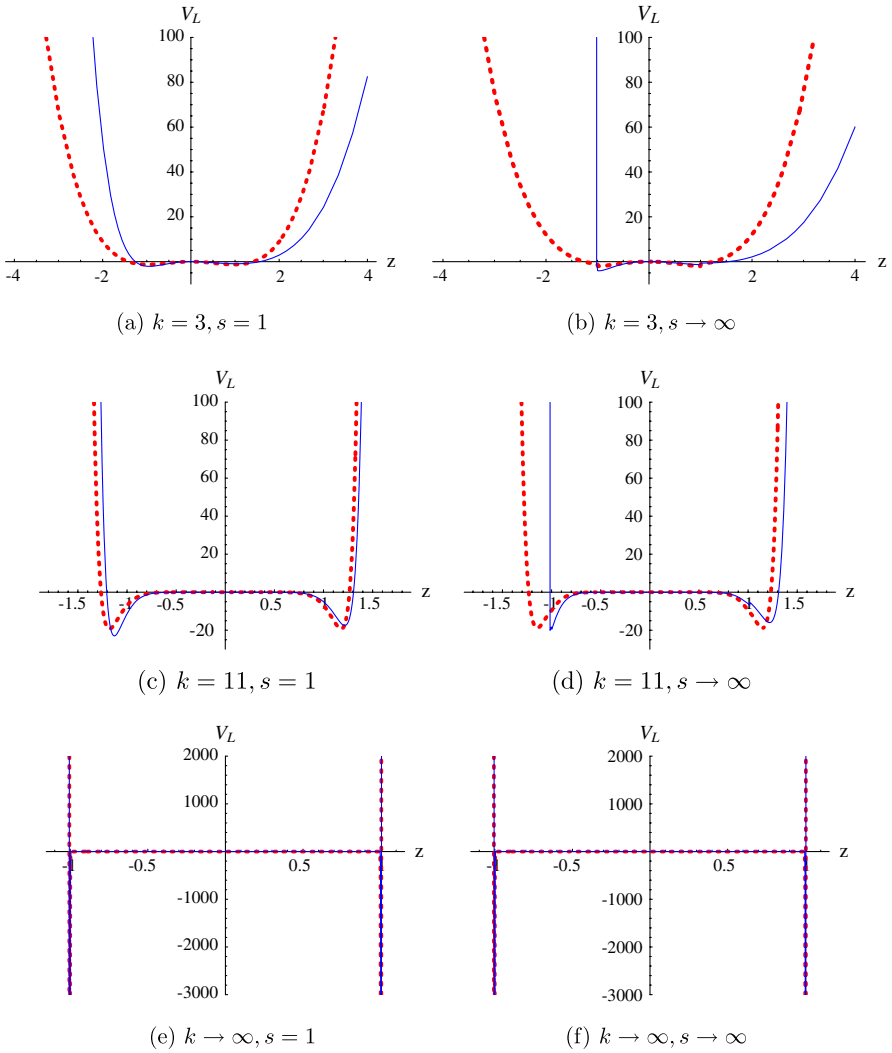

(a) $k = 3, s = 1$ (b) $k = 3, s \to \infty$

(c) $k = 11, s = 1$ (d) $k = 11, s \to \infty$

(e) $k \to \infty, s = 1$ (f) $k \to \infty, s \to \infty$

FIG. 19 (color online). Comparison of the asymmetric potential $V_L^A(z)$ (blue thin lines) with the symmetric potential $V_L^S(z)$ (red dashed lines) for the case $F(\phi) = \tan^{k/s}(\phi/\phi_0)$ with different k and s. The parameters are set to $\eta = \lambda = 1$, $a = 0$ for the red dashed lines and $a = 0.5$ for the blue thin lines, $s = 1$ and ∞, $k = 3$, 7, and ∞.

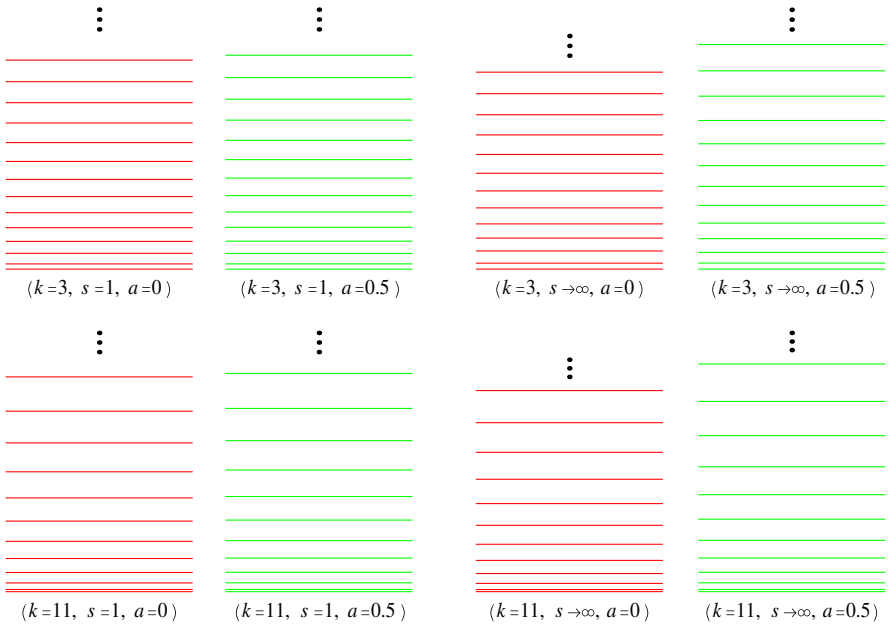

FIG. 20 (color online). Comparison of the spectra m^2_{Ln} of the asymmetric potential $V^A_L(z)$ ($a = 0.5$) with that of the symmetric potential $V^S_L(z)$ ($a = 0$) for the case $F(\phi) = \tan^{k/s}(\phi/\phi_0)$ with $k = 3$, 11 and $s = 1$, ∞. The parameters are set to $\eta = \lambda = 1$.

$$m^2_{Ln} = \{0, 1.59, 4.77, 8.50, 12.7, 17.4, 22.4, 27.7, 33.3, 39.2, 45.4, 51.7, \cdots\}, \qquad (s = 1) \tag{75}$$

$$m^2_{Ln} = \{0, 1.83, 5.09, 9.27, 14.0, 19.4, 25.2, 31.5, 38.2, 45.3, 52.7, 60.4, \cdots\}, \qquad (s \to \infty) \tag{76}$$

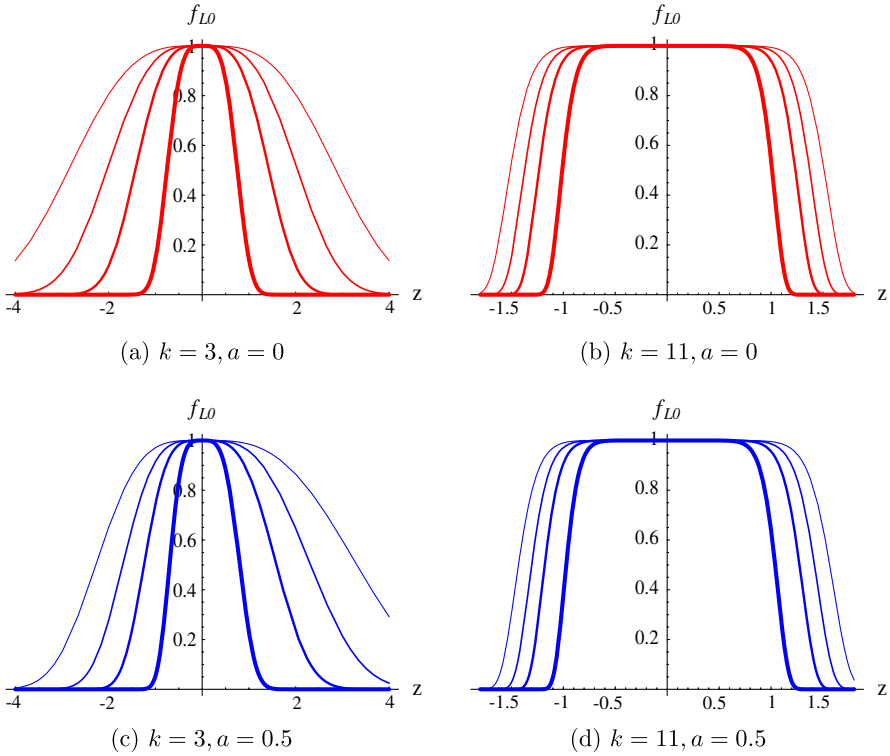

FIG. 21 (color online). Comparison of the zero modes of the asymmetric potential $V^A_L(z)$ (down two) with that of the symmetric potential $V^S_L(z)$ (up two) for the case $F(\phi) = \tan^{k/s}(\phi/\phi_0)$ with different k and η. The parameters are set to $s = 1$, $\lambda = 1$, $a = 0$, 0.5, $k = 3$, 11, $\eta = 0.1$, 0.3, 1, 10. The thickness of lines increases with η.

and

$$m_{Ln}^2 = \{0, 1.88, 7.40, 16.2, 28.1, 42.6, 59.8, 79.5, 102, 126, 153, 182, \cdots\}, \qquad (s = 1) \tag{77}$$

$$m_{Ln}^2 = \{0, 2.09, 8.22, 18.1, 31.4, 47.8, 67.5, 90.3, 116, 145, 177, 212, \cdots\}, \qquad (s \to \infty), \tag{78}$$

respectively, where $a = 0.5$, and the comparing with that of the symmetric potential is shown in Fig. 20. For $k \to \infty$, the difference between $V_L^A(z)$ and $V_L^S(z)$ disappears, and the spectrum is $m_{Ln} = n\lambda\pi/2 (n = 0, 1, 2, 3, \cdots)$.

The normalizable zero mode of left chiral fermions

$$f_{L0}(z) \propto \exp\left(\int^z d\bar{z} \frac{-\eta(\lambda\bar{z})^k[1 + (\lambda\bar{z})^{2s}]^{-(1/2s)}}{1 + a\bar{z}_2F_1(\frac{1}{2s}, \frac{1}{s}, 1 + \frac{1}{2s}, -(\lambda\bar{z})^{2s})}\right) \tag{79}$$

can also be localized on the brane without additional conditions. The effect of η, k, s, and the asymmetric factor a to the zero mode is shown in Figs. 21 and 22. It can be seen that, with the increase of η or k, the difference of zero modes with different a would reduce, i.e., the effect of the asymmetric factor could be neglected. While, with the increase of a, the effect of s cannot be neglected. For the case $a = 0.5$ and $s \to \infty$, our four-dimensional massless left fermions cannot appear in the range $z < -1/\lambda$ [see Fig. 22(d)], namely, the left sub-brane is the left boundary of the region that the four-dimensional massless left fermions could appear. The effect of k to the zero mode is remarkable: with the increase of k (i.e., the increase of the kink-fermion interaction), the region that the four-dimensional massless left fermions can appear would reduce. Especially, for the limit case $k \to \infty$, we have

$$f_{L0}(z) \propto \begin{cases} 1, & |\lambda z| < 1 \\ 0, & |\lambda z| > 1 \end{cases}, \tag{80}$$

which shows that the four-dimensional massless left fermions can only exist in between the locations of two sub-branes and the probability that they would appear is equal everywhere within the region.

IV. DISCUSSIONS AND CONCLUSIONS

In this paper, we have investigated the localization problem and the spectrum of spin half-fermions on a two-parameter (s and λ) family of symmetric branes and on a three-parameter (s, λ, and a) family of asymmetric thick branes in an AdS background for three kinds of typical kink-fermion couplings. The parameter a, which is called

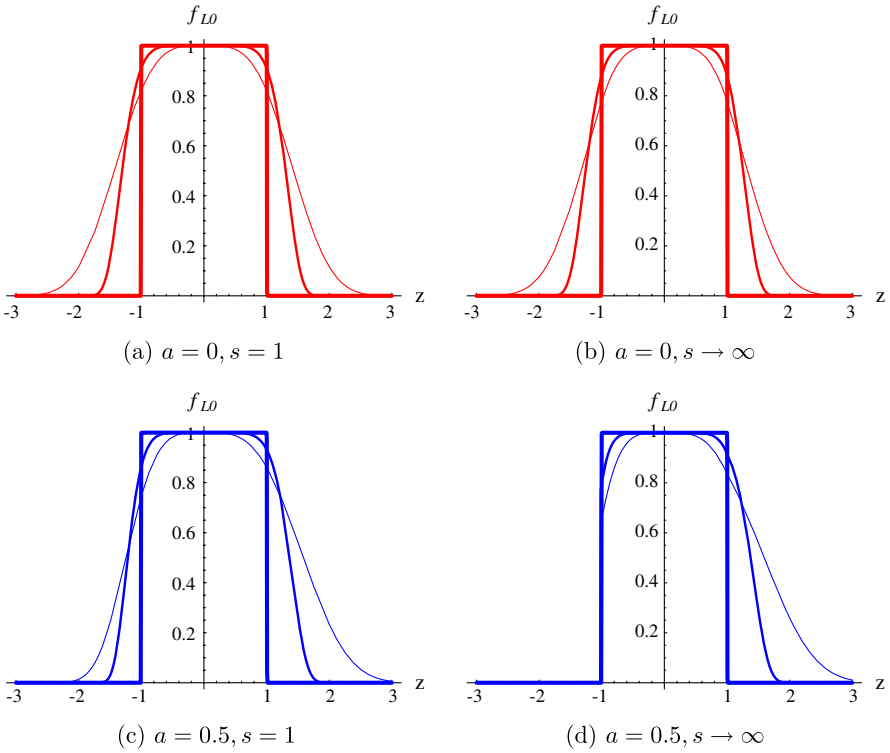

(a) $a = 0, s = 1$ (b) $a = 0, s \to \infty$

(c) $a = 0.5, s = 1$ (d) $a = 0.5, s \to \infty$

FIG. 22 (color online). Comparison of the zero modes of the asymmetric potential $V_L^A(z)$ (down two) with that of the symmetric potential $V_L^S(z)$ (up two) for the case $F(\phi) = \tan^{k/s}(\phi/\phi_0)$ with different k and s. The parameters are set to $\eta = \lambda = 1$, $k = 3$ for the thin lines, $k = 7$ for the thicker lines, and $k \to \infty$ for the thickest lines.

the asymmetry factor in this paper, decides the asymmetry of the solution. The parameter λ labels the thickness of the brane. For $s = 1$, the solution denotes an usual thick 1-brane, which is the regularized version of the Randall-Sundrum thin brane. For $a = 0$ ($a \neq 0$) and odd $s > 1$, the solution stands for a symmetric (an asymmetric) static double brane interpolating between the same (different) AdS_5 vacua. The thickness of the double brane is $2/\lambda$, the two sub-branes are localized at $z = \pm 1/\lambda$. The thickness of the sub-brane decreases with the increase of s. For the limit case $s \to \infty$, each thick sub-brane becomes a thin brane.

By presenting the mass-independent potentials (24) of KK modes in the corresponding Schrödinger equations, we investigate the localization and mass spectra of bulk fermions on the symmetric and asymmetric thick branes. The formation of the potentials (24) have two sources: the gravity-fermion coupling $\bar{\Psi}\Gamma^M\omega_M\Psi$ and the scalar-fermion coupling $-\eta\bar{\Psi}F(\phi)\Psi$. It can be seen that, without the gravity-fermion coupling, namely, only considering domain walls in a flat space-time, the potentials do not disappear and hence fermions could be localized on the domain walls (see, e.g., [1]). In fact, for a kink solution, it is clear that the potential for one of the left and right chiral fermions would be a PT-like potential, for which the massless mode of left or right chiral fermion can be localized on the domain wall without an additional condition. However, without scalar-fermion coupling ($\eta = 0$), there is no bound KK mode for both left and right chiral fermions. Hence, in order to localize the massless and massive left or right chiral fermions on the branes, some kind of Yukawa coupling should be introduced.

The spectra are determined by the behavior of the potentials at infinity. The potentials we are interested in have three types:

(1) $V_{L,R}(|z| \to \infty) \to 0$,
(2) $V_{L,R}(|z| \to \infty) \to C$,
(3) $V_{L,R}(|z| \to \infty) \to \infty$,

where C is a positive constant. In order to realize the three types of potentials, we have considered three typical Yukawa couplings correspondingly in this paper:
Case I "weak" interaction with $F(\phi) = \phi^k$ ($k \geq 1$),Case II "critical" interaction with $F(\phi) = \tan^{1/s}(\phi/\phi_0)$,Case III "strong" interaction with $F(\phi) = \tan^{k/s}(\phi/\phi_0)$ ($k > 1$).
Note that, as discussed above, for a domain wall solution in a flat space-time, a weak kink-fermion interaction would become a strong interaction. This means that the interaction with gravity would destroy the localization of fermions on the brane, in a way. So, the localization of fermions on the brane is the result of the competition of two interactions.

For the simplest Yukawa coupling with $F(\phi) = \phi$ and $\eta > 0$, the potentials for left chiral fermions provide no mass gap to separate the fermion zero mode from the excited KK modes. Provided the condition (39), the zero mode of left chiral fermions can be localized on the brane. The massless mode of left chiral fermion is easiest to be localized on the symmetric single brane (i.e., the $a = 0$ case). The asymmetric factor a may destroy the localization of massless fermions. For $s > 1$ (the double brane case), the potential for left chiral fermions has a double well at the location of the branes. The corresponding zero mode on both the symmetric and asymmetric double walls is essentially constant between the two interfaces. This is very different from the case of gravitons, scalars, and vectors, where the massless modes on the asymmetric double wall are strongly localized only on the interface centered around the lower minimum of the potential. The massive KK modes asymptotically turn into continuous plane waves when far away from the brane, which represent delocalized massive KK fermions. The massive modes with lower energy would experience an attenuation due to the presence of the potential barriers near the location of the brane. It is interesting to notice that, for $s \geq 3$, a potential well around the brane location for right chiral fermions would appear and the well becomes deeper and deeper with the increase of η. We have shown that this potential would result in a series of massive fermions with a finite lifetime [47,48]. The spectra of left-handed and right-handed fermionic resonances are the same, which demonstrates that a Dirac fermion could be composed from the left and right resonance KK modes [48].

For the critical interaction with $F(\phi) = \tan^{1/s}(\phi/\phi_0)$ and $\eta > 0$, we get a PT-like potential for left chiral fermions, which provides a mass gap to separate the zero mode from the excited KK modes. The mass spectra for left and right chiral fermions are almost the same, and the only one difference is the absence of the zero mode of right chiral fermions. The massless KK mode of left chiral fermions is normalizable without additional conditions, and it would be strongly localized on the brane with the large coupling constant η. The massive bound KK modes would appear provided large η. The spectra for the single brane and the double brane are quite different. For large η, there are more bound massive KK modes on the single brane than on the double brane. For the double thin brane ($s \to \infty$), a harmonic oscillator potential well with finite depth will get for both left and right chiral fermions and there are finite bound KK modes. For the asymmetric brane case, the potentials $V^S_{L,R}(z)$ are enlarged at $z \to +\infty$ and diminished at $z \to -\infty$, which shows that the asymmetric factor would reduce the number of the bound KK modes of left and right fermions. The continuous spectrum starts at different values for different s. The spectrum structure for the single brane case ($s = 1$) is dramatically changed by the asymmetric factor: the number of bound KK modes quickly decreases with the increase of a and the difference with the double brane case is reduced.

For the strong interaction with $F(\phi) = \tan^{k/s}(\phi/\phi_0)$ ($k > 1$), the potentials $V^{S,A}_{L,R}(z)$ trend to infinite when far

away from the brane and vanish at $z = 0$, and there exist infinite discrete bound KK modes. The influence of s is not important for symmetric potentials $V^S_{L,R}(z)$, which indicates that the spectra on the single brane and the double brane are almost the same. While the increase of k will dramatically change the shape of the potentials, especially for $k \to \infty$, the potential for right hand fermions is an infinite deep square well. For a fixed finite k, the difference of the symmetric and asymmetric potentials would become large with the increase of s. For $s \to \infty$, the difference is the largest. While for a fixed s, the difference of the two potentials would become small with the increase of k. The normalizable zero mode of left chiral fermions can also be localized on the brane without additional conditions. With the increase of η or k, the effect of the asymmetric factor to the zero mode can be neglected. While, with the increase of a, the effect of s is obvious. For the limit case $s \to \infty$, the left sub-brane is the left boundary of the region that the four-dimensional massless left fermions could appear. With the increase of k, the region that the four-dimensional massless left fermions can appear would reduce. Especially, for the limit case $k \to \infty$, the four-dimensional massless left fermions can only exist in between the locations of two sub-branes with equal probability.

ACKNOWLEDGMENTS

This work was supported by the Program for New Century Excellent Talents in University, the National Natural Science Foundation of China (No. 10705013), the Doctoral Program Foundation of Institutions of Higher Education of China (No. 20070730055), and the Key Project of Chinese Ministry of Education (No. 109153).

[1] V. A. Rubakov and M. E. Shaposhnikov, Phys. Lett. **125B**, 136 (1983); **125B**, 139 (1983).
[2] K. Akama, Lect. Notes Phys. **176**, 267 (1983); C. Wetterich, Nucl. Phys. **B253**, 366 (1985); S. Randjbar-Daemi and C. Wetterich, Phys. Lett. **166B**, 65 (1986).
[3] N. Arkani-Hamed, S. Dimopoulos, and G. Dvali, Phys. Lett. B **429**, 263 (1998); I. Antoniadis, N. Arkani-Hamed, S. Dimopoulos, and G. Dvali, Phys. Lett. B **436**, 257 (1998).
[4] L. Randall and R. Sundrum, Phys. Rev. Lett. **83**, 3370 (1999); **83**, 4690 (1999).
[5] J. Lykken and L. Randall, J. High Energy Phys. 06 (2000) 014.
[6] S. Randjbar-Daemi and M. E. Shaposhnikov, Phys. Lett. B **491**, 329 (2000); T. Gherghetta and A. Kehagias, Phys. Rev. Lett. **90**, 101601 (2003).
[7] G. D. Starkman, D. Stojkovic, and M. Trodden, Phys. Rev. D **63**, 103511 (2001); Phys. Rev. Lett. **87**, 231303 (2001).
[8] R. Koley, J. Mitra, and S. SenGupta, Phys. Rev. D **76**, 064030 (2007); **79**, 041902(R) (2009).
[9] W. D. Goldberger and M. B. Wise, Phys. Rev. Lett. **83**, 4922 (1999).
[10] O. DeWolfe, D. Z. Freedman, S. S. Gubser, and A. Karch, Phys. Rev. D **62**, 046008 (2000).
[11] M. Gremm, Phys. Lett. B **478**, 434 (2000).
[12] M. Gremm, Phys. Rev. D **62**, 044017 (2000); K. Ghoroku and M. Yahiro, arXiv:hep-th/0305150; A. Kehagias and K. Tamvakis, Mod. Phys. Lett. A **17**, 1767 (2002); Phys. Lett. B **504**, 38 (2001); M. Giovannini, Phys. Rev. D **64**, 064023 (2001); **65**, 064008 (2002); S. Kobayashi, K. Koyama, and J. Soda, Phys. Rev. D **65**, 064014 (2002).
[13] C. Csaki, J. Erlich, T. Hollowood, and Y. Shirman, Nucl. Phys. **B581**, 309 (2000).
[14] A. Campos, Phys. Rev. Lett. **88**, 141602 (2002).
[15] R. Emparan, R. Gregory, and C. Santos, Phys. Rev. D **63**, 104022 (2001); A. Wang, Phys. Rev. D **66**, 024024 (2002); A. Melfo, N. Pantoja, and A. Skirzewski, Phys. Rev. D **67**, 105003 (2003); K. A. Bronnikov and B. E. Meierovich, Gravitation Cosmol. **9**, 313 (2003); O. Castillo-Felisola, A. Melfo, N. Pantoja, and A. Ramirez, Phys. Rev. D **70**, 104029 (2004); M. Minamitsuji, W. Naylor, and M. Sasaki, Nucl. Phys. **B737**, 121 (2006).
[16] R. Guerrero, A. Melfo, and N. Pantoja, Phys. Rev. D **65**, 125010 (2002).
[17] V. Dzhunushaliev, V. Folomeev, D. Singleton, and S. Aguilar-Rudametkin, Phys. Rev. D **77**, 044006 (2008); V. Dzhunushaliev, V. Folomeev, K. Myrzakulov, and R. Myrzakulov, Gen. Relativ. Gravit. **41**, 131 (2009).
[18] D. Bazeia, F. A. Brito, and J. R. Nascimento, Phys. Rev. D **68**, 085007 (2003); D. Bazeia, C. Furtado, and A. R. Gomes, J. Cosmol. Astropart. Phys. 02 (2004) 002; D. Bazeia, F. A. Brito, and A. R. Gomes, J. High Energy Phys. 11 (2004) 070; D. Bazeia and A. R. Gomes, J. High Energy Phys. 05 (2004) 012; D. Bazeia, F. A. Brito, and L. Losano, J. High Energy Phys. 11 (2006) 064; D. Bazeia, A. R. Gomes, and L. Losano, Int. J. Mod. Phys. A **24**, 1135 (2009).
[19] Y. Shtanov, V. Sahni, A. Shafieloo, and A. Toporensky, J. Cosmol. Astropart. Phys. 04 (2009) 023; K. Farakos, N. E. Mavromatos, and P. Pasipoularides, arXiv:0902.1243; M. Sarrazin and F. Petit, arXiv:0903.2498; V. Dzhunushaliev, V. Folomeev, and M. Minamitsuji, Phys. Rev. D **79**, 024001 (2009).
[20] V. Dzhunushaliev, V. Folomeev, and M. Minamitsuji, arXiv:0904.1775.
[21] T. R. Slatyer and R. R. Volkas, J. High Energy Phys. 04 (2007) 062; R. Davies, D. P. George, and R. R. Volkas, Phys. Rev. D **77**, 124038 (2008).
[22] S. L. Parameswaran, S. Randjbar-Daemi, and A. Salvio, Nucl. Phys. **B767**, 54 (2007).
[23] Y. X. Liu, L. Zhao, and Y. S. Duan, J. High Energy Phys. 04 (2007) 097; L. Zhao, Y.-X. Liu, and Y.i-S. Duan, Mod.

Phys. Lett. A **23**, 1129 (2008).
[24] G. de Pol, H. Singh, and M. Tonin, Int. J. Mod. Phys. A **15**, 4447 (2000).
[25] Y. X. Liu, L. Zhao, X. H. Zhang, and Y. S. Duan, Nucl. Phys. **B785**, 234 (2007).
[26] Y. Q. Wang, T. Y. Si, Y. X. Liu, and Y. S. Duan, Mod. Phys. Lett. A **20**, 3045 (2005); Y. S. Duan, Y. X. Liu, and Y. Q. Wang, Mod. Phys. Lett. A **21**, 2019 (2006); Y. X. Liu, Y. Q. Wang, and Y. S. Duan, Commun. Theor. Phys. **48**, 675 (2007).
[27] S. Rafael and S. Torrealba, arXiv:0803.0313.
[28] G. Starkman, D. Stojkovic, and T. Vachaspati, Phys. Rev. D **65**, 065003 (2002); **63**, 085011 (2001); D. Stojkovic, Phys. Rev. D **63**, 025010 (2000).
[29] S. Randjbar-Daemi and M. Shaposhnikov, Phys. Lett. B **492**, 361 (2000).
[30] O. Arias, R. Cardenas, and I. Quiros, Nucl. Phys. **B643**, 187 (2002).
[31] N. Barbosa-Cendejas and A. Herrera-Aguilar, J. High Energy Phys. 10 (2005) 101.
[32] N. Barbosa-Cendejas and A. Herrera-Aguilar, Phys. Rev. D **73**, 084022 (2006).
[33] X.-H. Zhang, Y.-X. Liu, and Y.-S. Duan, Mod. Phys. Lett. A **23**, 2093 (2008); Y.-X. Liu, X.-H. Zhang, L.-D. Zhang, and Y.-S. Duan, J. High Energy Phys. 02 (2008) 067.
[34] D. Bazeia, F. A. Brito, and R. C. Fonseca, arXiv:0809.3048; P. Koroteev and M. Libanov, Phys. Rev. D **79**, 045023 (2009); A. Flachi and M. Minamitsuji, Phys. Rev. D **79**, 104021 (2009).
[35] N. Barbosa-Cendejas, A. Herrera-Aguilar, M. A. Reyes, and C. Schubert, Phys. Rev. D **77**, 126013 (2008); N. Barbosa-Cendejas, A. Herrera-Aguilar, U. Nucamendi, and I. Quiros, arXiv:0712.3098.
[36] Y.-X. Liu, L.-D. Zhang, S.-W. Wei, and Y.-S. Duan, J. High Energy Phys. 08 (2008) 041.
[37] Y. Kodama, K. Kokubu, and N. Sawado, Phys. Rev. D **79**, 065024 (2009); Y. Brihaye and T. Delsate, Phys. Rev. D **78**, 025014 (2008).
[38] S. L. Dubovsky, V. A. Rubakov, and P. G. Tinyakov, Phys. Rev. D **62**, 105011 (2000).
[39] R. Koley and S. Kar, Classical Quantum Gravity **22**, 753 (2005).
[40] Y.-X. Liu, Z.-H. Zhao, S.-W. Wei, and Y.-S. Duan, J. Cosmol. Astropart. Phys. 02 (2009) 003.
[41] R. Guerrero, A. Melfo, N. Pantoja, and R. O. Rodriguez, Phys. Rev. D **74**, 084025 (2006); A. Melfo, N. Pantoja, and J. D. Tempo, Phys. Rev. D **73**, 044033 (2006).
[42] R. Guerrero, R. O. Rodriguez, and R. Torrealba, Phys. Rev. D **72**, 124012 (2005).
[43] A. Melfo, N. Pantoja, and A. Skirzewski, Phys. Rev. D **67**, 105003 (2003).
[44] R. Gregory and A. Padilla, Phys. Rev. D **65**, 084013 (2002).
[45] D. Bazeia, C. Furtado, and A. R. Gomes, J. Cosmol. Astropart. Phys. 02 (2004) 002.
[46] Y.-X. Liu, L.-D. Zhang, L.-J. Zhang, and Y.-S. Duan, Phys. Rev. D **78**, 065025 (2008).
[47] C. A. S. Almeida, M. M. Ferreira, Jr., A. R. Gomes, and R. Casana, Phys. Rev. D **79**, 125022 (2009).
[48] Y.-X. Liu, J. Yang, Z.-H. Zhao, C.-E. Fu, and Y.-S. Duan, Phys. Rev. D **80**, 065019 (2009).
[49] R. Gregory, V. A. Rubakov, and S. M. Sibiryakov, Phys. Rev. Lett. **84**, 5928 (2000).